2019-11-26

An integrated approach to determine interactive genotoxic and global gene expression effects of multiwalled carbon nanotubes (MWCNTs) and benzo[a]pyrene (BaP) on marine mussels: evidence of reverse 'Trojan Horse' effects

Barranger, A

10.1080/17435390.2019.1654003
Nanotoxicology
Informa UK Limited

An integrated approach to determine interactive genotoxic and global gene expression effects of multiwalled carbon nanotubes (MWCNTs) and Benzo[*a*]pyrene (BaP) on marine mussels: Evidence of reverse 'Trojan Horse' effects

Audrey Barranger[a†], Graham A. Rance[b,c], Yann Aminot[d], Lorna J. Dallas[a], Susanna Sforzini[e], Nicola J. Weston[c], Rhys W. Lodge[b,c], Mohamed Banni[e,f], Volker M. Arlt[g,h], Michael N. Moore[a,i,j], James W. Readman[d,i], Aldo Viarengo[e], Andrei N. Khlobystov[b,c], Awadhesh N. Jha[a*]

[a]School of Biological and Marine Sciences, University of Plymouth, PL4 8AA Plymouth, United Kingdom; [b]School of Chemistry, University of Nottingham, University Park, NG7 2RD Nottingham, UK; [c]Nanoscale and Microscale Research Centre, University of Nottingham, NG7 2RD Nottingham, UK; [d]Centre for Chemical Sciences, University of Plymouth, PL4 8AA Plymouth, United Kingdom; [e]Ecotoxicology and Environmental Safety Unit, Istituto di Ricerche Farmacologiche Mario Negri IRCCS, Via Giuseppe La Masa 19, 20156 Milan, Italy; [f]Laboratory of Biochemistry and Environmental Toxicology, ISA chottMariem, Sousse University, Sousse, Tunisia; [g]Department of Analytical, Environmental and Forensic Sciences, King's College London, MRC-PHE Centre for Environmental & Health, SE1 9NH London, United Kingdom; [h]NIHR Health Protection Research Unit in Health Impact of Environmental Hazards at King's College London in partnership with Public Health England and Imperial College London, SE1 9NH London, United Kingdom; [i]Plymouth Marine Laboratory, Prospect Place, The Hoe, PL1 3HD Plymouth, United Kingdom; [j]European Centre for Environment & Human Health (ECEHH), University of Exeter Medical School, Knowledge Spa, Royal Cornwall Hospital, TR1 3LJ Truro, Cornwall, United Kingdom

Running Title: *Interactive effects of multiwalled carbon nanotubes (MWCNTs) and Benzo[a] pyrene (BaP) on marine mussels*

*Correspondence: Awadhesh N. Jha, School of Biological and Marine Sciences, University of Plymouth, Plymouth, PL4 8AA, UK. E-mail: a.jha@plymouth.ac.uk/

[†]Present address: Université de Rennes 1 / Centre National de la Recherche Scientifique, UMR 6553 ECOBIO, Rennes, F-35000, France

An integrated approach to determine interactive genotoxic and global gene expression effects of multiwalled carbon nanotubes (MWCNTs) and Benzo[a] pyrene (BaP) on marine mussels: Evidence of reverse 'Trojan Horse' effects

Abstract

The interactions between carbon-based engineered nanoparticles (ENPs) and organic pollutants might enhance the uptake of contaminants into biota. The present integrated study aimed to assess this potential 'Trojan Horse', probing the interactive effects of purpose-made multi-walled carbon nanotubes (MWCNTs), a representative ENP, and benzo[*a*]pyrene (BaP), a ubiquitous polycyclic aromatic hydrocarbon (PAH) pollutant, on the marine mussel *Mytilus galloprovincialis.* Mussels were exposed to MWCNTs and BaP either alone or in various combinations. The co-exposure of BaP with MWCNTs revealed that the presence of MWCNTs enhanced the aqueous concentrations of BaP, thereby reducing the uptake of this pollutant by mussels as evidenced by lowering BaP concentrations in the tissues. Determination of DNA damage (comet assay) showed a concentration- dependent response for BaP alone which was absent when MWCNTs were present. Global gene expression using microarray analyses indicated that BaP and MWCNTs, in combination, differentially activated those genes which are involved in DNA metabolism compared to the exposures of BaP or MWCNTs alone, and the gene expression response was tissue-specific. Mechanisms to explain these results are discussed and relate primarily to the adsorption of BaP on MWCNTs, mediated potentially by van der Waals interactions. The use of a novel approach based on gold-labelled MWCNTs to track their uptake in tissues improved the traceability of nanotubes in biological samples. Overall, our results did not indicate the 'Trojan Horse' effects following co-exposure to the contaminants and clearly showed that the adsorption of BaP to MWCNTs modified the uptake of the pollutant in marine mussels.

Keywords: *Mytilus galloprovincialis*; benzo[*a*]pyrene; multi-walled carbon nanotubes; van der Waals interactions; adsorption

Introduction

The production of manufactured or engineered nanoparticles (ENPs) and nanomaterials (NMs) has grown extensively over the last few years and they are entering into the environment (Giese *et al.*, 2018). Both academic and industrial researchers are extensively exploring their unusual, size-dependent properties to develop the next generation of functional materials. The research effort has led to the exploration of a number of promising applications of ENPs and NMs, particularly in the health sector, where their potential utilisation as targeted drug delivery agents are being investigated (Cho *et al.* 2008). However, to date most of the actual applications of ENPs and NMs are associated with consumer products, e.g. in cosmetics, food and food packaging, paints and coatings (Foss Hansen *et al.* 2016). In fact, in January 2019, it was reported that more than 3,000 products in Europe alone contained NPs and NMs, with the database having grown by 1,000 products over the course of just 18 months (Foss Hansen *et al.* 2016; http://nanodb.dk/). Yet, whilst the benefits and improvements offered by nanotechnology are well established, significant concern regarding the potential risks have been raised. This stems from the fact that nanoscale materials, in common with other pollutants, can enter the aquatic environment through different routes (Giese *et al.*, 2018) with very little research to assess their potential impact on human health and the natural environment established.

Among ENPs, carbon-based nanoparticles, especially carbon nanotubes (CNTs), are of major commercial interest, currently incorporated in a diverse range of commercial products, from rechargeable batteries and automotive parts to sporting goods and in water filters (DeVolder *et al.* 2013). CNTs have the highest production volumes among engineered carbonaceous nanomaterials worldwide (Gottschalk *et al.* 2013), exceeding 730 tonnes per year in Europe (Sun *et al.* 2016). Based on this production data, the latest predictions estimate the environmental concentrations of CNTs in surface water at 0.28 ng L^{-1} ($Q_{0.15}$ = 0.04 ng L^{-1}; $Q_{0.85}$ = 0.65 ng L^{-1}) (Sun *et al.* 2016). With a substantial rise in the production and use of CNTs expected over the coming years, the concentrations of CNTs in all environmental compartments, including the aquatic environment, will inevitably increase. Of particular concern are multi-walled carbon nanotubes (MWCNTs) as they are presently used to reduce the biofouling of ship hulls by discouraging the attachment of algae and barnacles (Beigbeder *et al.* 2008) and hence are directly released into the marine environment.

Whilst the presence of nanoscale materials in seawater represents a significant current issue, it is, in fact, their potential combination with other ubiquitous contaminants that represents a far more pressing concern. Carbon nanotubes, possessing a large hydrophobic surface area, have a high adsorption capacity for hydrophobic molecules and thus a high affinity for co-released environmental pollutants. Among these contaminants, polycyclic aromatic hydrocarbons (PAHs) represent a significant concern. One of them, benzo[*a*]pyrene (BaP), is a known mutagenic and carcinogenic contaminant, present in human foods as well as being ubiquitous in environmental samples (Sogbanmu *et al.* 2016, Acevedo-Whitehouse *et al.* 2018; Di *et al.*, 2011). It is on the list of the priority pollutants of the European Water Framework Directive (2000/60/CE) and is also a monitored PAH of the United States Environmental Protection Agency (USEPA). To date, few studies have investigated the interactive effects of carbon-based nanoparticles with different environmental pollutants on aquatic organisms, especially marine organisms, with significant inconsistencies in the results reported (reviewed in Canesi *et al.* 2015; Barranger *et al.*, 2019). Indeed, available data on the combined effects of CNTs and other contaminants in aquatic organisms are inconclusive, if not conflicting. Some studies indicate that the adsorption of pollutants to CNTs reduces their bioaccumulation in organisms (Ferguson *et al.* 2008), whereas others highlight that co-exposure with

CNTs may amplify the toxic effects of other compounds by increasing their cellular uptake and accumulation (Sun *et al.* 2014). These conflicting results could be explained by current evidence suggesting that the variability in bioavailability of CNT-adsorbed organic contaminants is largely driven by the size, configuration and surface area coverage of the contaminant on the nanomaterial (Linard *et al.* 2017).

In addition to conflicting genotoxicological studies, one of the major challenges that has limited the investigation of CNT uptake in environmental studies is the lack of a method to quantify them in biological or environmental media. A recent review (Bjorkland *et al.* 2017) highlighted that CNTs have been detected in environmental matrices and organisms using a broad range of analytical techniques, including optical spectroscopies, electron microscopy, thermal methods and radiolabelling. However, these methods are generally qualitative or at best quantitative with some bias and do not precisely determine the concentration of CNTs in organisms.

With knowledge of the above information, in this study, we evaluated the interactions between MWCNTs and the ubiquitous environmental pollutant BaP on marine mussels. Firstly, we analysed the aggregation properties and genotoxicity of MWCNTs using light scattering and two different assays (the comet and the micronucleus assays), respectively. Secondly, in a series of experiments where mussels were co-exposed to MWCNTs and BaP at different concentrations, we measured the uptake, expression of genes related to DNA metabolism as well as DNA damage and bulky DNA adduct formation in mussels. Finally, we probed the novel application of gold-labelled MWCNTs as a method to improve the tracking of carbon nanotubes in mussel tissues, utilising both spectroscopy and electron microscopy approaches. This integrated and interdisciplinary strategy allowed us to test whether the combination of BaP with MWCNTs induces molecular pathways different to those observed for the pollutant alone and thus the viability of MWCNTs as a potential 'Trojan Horse' effects.

Materials and Methods

Mussel collection and maintenance

Mussels (*Mytilus galloprovincialis*; 45-50 mm) collected from the intertidal zone at Trebarwith Strand, Cornwall, a reference site (50° 38' 40" N, 4° 45' 44" W) were maintained under laboratory conditions prior to experimentations as described previously (Dallas *et al.* 2013, D'Agata *et al.* 2014, Vernon and Jha 2019).

Preparation and characterisation of MWCNTs

MWCNTs were purchased from NanoLab, USA (PD30L520, synthesised by chemical vapour deposition). In the absence of a single Organisation for Economic Cooperation and Development (OECD) standard for MWCNTs (OECD Environmental, Health and Safety Publications Dossier No. 68), these MWCNTs were selected owing to their structural and physicochemical similarities to other MWCNTs commonly reported in the wider literature. Moreover, the study of MWCNTs, rather than single-walled carbon nanotubes (SWCNTs), was deemed more imperative given their greater commercial application and thus propensity to be released into the natural environment. To homogenise the nanotube length distribution, MWCNTs were shortened and purified using a multi-step strategy based on site-selective catalytic oxidation (LaTorre *et al.* 2010, Miners *et al.* 2014). In

studies on bivalve molluscs, ENPs and NMs are typically characterised in seawater without animals (Gomes *et al.* 2013, D'Agata *et al.* 2014), which is not strictly speaking representative of the experimental conditions. In order to better replicate the conditions of the experiment during analysis, mussels (4.5 mussels L^{-1}) were maintained in 2-L glass beakers for 24 h with natural seawater from Plymouth Sound (filtered at 10 µm). Subsequently, MWCNTs (1 mg) were added to the mussel-exposed seawater (10 mL) and the suspension homogenised by ultrasonication (Langford Sonomatic 375, 40 kHz) for 1 h at room temperature. The suspension was allowed to settle for at least 4 h at room temperature prior to analysis of the aggregate size. Control measurements of aggregate size in (i) seawater, in the absence of mussels and (ii) mussel-exposed seawater in the presence of BaP (1 mg L^{-1}) were additionally performed. Dynamic light scattering (DLS) was performed using a Malvern Zetasizer Nano-ZS at room temperature. Quoted values are the average of 2-3 measurements. Bright field transmission electron microscopy (TEM) was performed using the JOEL 2100+ microscope operated at 200 keV. Energy dispersive X-ray (EDX) spectra were acquired using an Oxford Instruments INCA X-ray microanalysis system and processed using Aztec software. Samples were prepared by casting several drops of the respective suspensions onto copper grid-mounted lacey carbon films.

Exposure of Mytilus galloprovincialis to MWCNTs

Experimental design

After depuration, the mussels were transferred to 2-L glass beakers containing 1.8 L of the same seawater as above and allowed to acclimatise for 48 h. Two mussels were used per beaker. A photoperiod of 12 h light, 12 h dark was maintained throughout the experiment. Good seawater oxygenation was provided by a bubbling system. The seawater quality was monitored in each of the beakers by measuring the salinity (36.65 ± 0.18‰), pH (7.98 ± 0.04), percentage of dissolved oxygen (97.09 ± 1.28%) and temperature (14.89 ± 0.13°C). Mussels were exposed to different treatments for 7 days: a seawater control (12 mussels); a positive control (0.04 mg L^{-1} CuSO4; 12 mussels); 0.01 mg L^{-1} MWCNTs (12 mussels); 0.1 mg L^{-1} MWCNTs (12 mussels); and 1 mg L^{-1} MWCNTs (12 mussels). MWCNTs were pre-weighed in glass vials for each beaker according to the required final concentration (0.018 mg, 0.18 mg and 1.8 mg to reach 0.01, 0.1 and 1 mg L^{-1} respectively) and directly tipped in the beakers. Mussels were not fed and did not spawn during the experiment. At the end of the exposure, 10 mussels were sampled for each treatment. Two different tissues, gills and digestive gland (DG) were used to perform the comet assay and the micronucleus assay. Gill and digestive gland cells were chosen to unravel the potential interactive toxic effects of MWCNTs and BaP. In mussels, feed particles are filtrated first through gills and transported up to the digestive gland (DG) to be metabolized. This leads to high bioaccumulation of contaminants in this tissue. It is to be noted that as an analogue to mammalian liver, enzymes involved in the biotransformation of both endogenous and exogenous substrates are mainly localized in the digestive gland of mussels (Livingstone and Pipe 1992, Akcha *et al.* 1999).

Comet assay to determine DNA damage

The comet assay on gill and digestive gland (DG) cells (n = 10) was performed as previously described by us (Dallas *et al.* 2013, Banni *et al.* 2017, Vernon and Jha 2019).

Micronucleus assay

For the micronucleus assay, tissues (i.e. gill and DG) were digested with the same protocol as for the comet assay. The cell suspension was spread gently across the slide with a clean cover slip, allowed to adhere onto the slides by placing in the fridge for 1 h. To fix the cells, the dried slides were immersed in a coupling jar containing Carnoy's fixative for 20 min. Following fixation, the slides were stained with 20µl of ethidium bromide (20 µg mL^{-1}). Slides were randomised and scored under the microscope for the induction of micronuclei. At least 1000 cells were scored from each slide (two slides per individual mussel) according to the detailed criteria described elsewhere (Bolognesi and Fenech 2012, Dallas *et al.* 2013, Vernon and Jha 2019).

Exposure of *Mytilus galloprovincialis* to BaP and MWCNTs

Experimental design

In a separate experiment, mussels were exposed for 3 days (with no water changes) to BaP alone (5, 50 and 100 µg L^{-1}), MWCNTs alone (1 mg L^{-1}) and a combination of BaP and MWCNTs (1 mg L^{-1} MWCNTs + 5 µg L^{-1} BaP; 1 mg L^{-1} MWCNTs + 50 µg L^{-1} BaP; 1 mg L^{-1} MWCNTs + 100 µg L^{-1} BaP). Concurrently, mussels were also exposed to a solvent control (0.02% DMSO). Due to the chemical composition of seawater, the occurrence of PAHs (very hydrophobic compounds), is at very low levels (<1 ng/L), in contrast to concentration in other aqueous matrices. For example, in marine sediments, the corresponding values could be in the range of 1 ng/g d.w. to >10000 ng/g d.w. (Nikolaou *et al.* 2009). In marine mussels, depending on the study area, PAHs can be found at concentrations ranging from 25 to 3 900 ng/g d.w. (Baumard *et al.* 1998, 1999), corresponding to our lowest exposure concentration (5µg.L^{-1}). Regarding the selection of higher BaP exposure concentrations (50 and 100 µg.L^{-1}), previous studies have reported that the selected concentration-range induced biological or biomarker responses in mussels (Halldórsson *et al.* 2008, Di *et al.* 2011, Banni *et al.* 2017). In the present study, for each treatment, 26 mussels were used. As previously described, MWCNTs were pre-weighed in glass vials for each beaker according to the final concentration (1.8 mg to reach 1 mg L^{-1}) and directly tipped into the beakers. Seawater quality was monitored in each of the beakers by measuring the salinity (36.42 ± 0.05‰), pH (7.72 ± 0.11), percentage of dissolved oxygen (94.58 ± 2.40%) and temperature (15.55 ± 0.32°C).

Chemical analysis of BaP in water and tissue

Water and tissue extracts were analysed using an Agilent Technologies (Stockport, UK) 7890A Gas Chromatography (GC) system interfaced with an Agilent 5975 series Mass Selective (MS) detector as described previously by us (Banni *et al.* 2017).

DNA metabolism gene expression

Microarray hybridisation and analysis. Competitive dual-colour microarray hybridisation was performed with the STREM (Stress Response Microarray in *Mytilus sp.*) platform (Banni *et al.* 2017); fluorescence-labelled cDNA probes were obtained by direct labelling in the presence of modified Cy3- and Cy5-dCTP (Perkin Elmer). The procedure was carried out as described previously (Banni *et al.* 2011, 2017). MIAMI-compliant microarray data, including a detailed description of the experimental design

and each hybridization experiment, were deposited in the Gene Expression Omnibus (http://www.ncbi.nlm.nih.gov/geo/query/).

Functional genomics analysis

Functional characterisation of mussel genes represented on a microarray was based on Gene Ontology (GO) annotation and carried out in Blast2GO (Conesa *et al.* 2005) using default parameters. However, in the case of the STREM platform, target genes were putatively annotated and ranked under established biological processes, making the generation of robust processes easier and faster.

qRT-PCR. qRT-PCR analysis was carried out using the same RNA extracted for microarray hybridization. Relative mRNA abundance of the mussel genes encoding 4 Probes and primer pairs (Table S2) were designed using Beacon Designer v3.0 (Premier Biosoft International, Inc.). The procedure is described in (Banni *et al.* 2011, 2017).

Comet assay

The comet assay was performed as reported above (section "Comet assay to determine DNA damage") with gills and DG tissues from 10 mussels for each treatment.

DNA adducts

DNA from 10 mussels for each treatment was isolated from gills and DG tissues using a standard phenol-chloroform extraction procedure. We used the nuclease P1 enrichment version of the thin-layer chromatography (TLC) ^{32}P-postlabelling assay to detect BaP-derived DNA adducts (i.e. 10-(deoxyguanosin-N^2-yl)7,8,9-trihydroxy-7,8,9,10-tetrahydro-BaP [dG-N^2-BPDE]). The procedure was essentially performed as described previously (Phillips and Arlt 2014).

Evaluation of the uptake of gold-labelled MWCNTs by mussels

Synthesis of labelled nanotubes

To probe the uptake of carbon nanotubes by the mussels, it was necessary to label the nanotubes with a diagnostic marker. Gold was selected for this purpose due to its relatively low abundance in the natural environment (Goldberg 1987), thus providing an excellent spectroscopic handle facilitating ease of detection by both bulk and local-probe spectroscopy approaches. Confinement of nanoparticles within the internal void of MWCNTs is a highly efficient process allowing retention of the metal label in the system (Miners *et al.* 2016) and simultaneously excluding any interference of the label with measurements on nanotubes. Gold nanoparticles were synthesised using a modified Brust-Schiffrin reduction (Rance *et al.* 2008) followed by insertion into MWCNTs utilising a thermally-assisted Ostwald ripening procedure yielding AuNP@MWCNTs (Scheme S1).

Experimental design

Mussels were exposed to labelled MWCNTs only (1 mg L^{-1} AuNP@MWCNTs) and in combination with

BaP as the same concentration as above (1 mg L^{-1} AuNP@MWCNTs + 5 µg L^{-1} BaP; 1 mg L^{-1} AuNP@MWCNTs + 50 µg L^{-1} BaP; 1 mg L^{-1} AuNP@MWCNTs + 100 µg L^{-1} BaP). Four mussels were used for each treatment.

Bulk spectroscopic analysis

For the determination of tissue-specific gold concentration, 4 mussels per treatment were analysed by inductively coupled plasma mass spectrometry (ICP-MS). Each individually dissected tissue (gills, DG, all other tissues pooled together) was washed with distilled water, blotted dry and transferred to a pre-weighed acid washed vial. Samples were dried overnight at 60°C and re-weighed. Tissue digestion was achieved by addition of 1 mL concentrated nitric acid (trace analysis grade) and incubation for 2 h at 70°C. Digested tissue samples were diluted to a final volume of 5 mL with Millipore Milli Q water and stored at room temperature until analysis. An internal standard of 115-In was added, to a final concentration of 10 µg L^{-1}. This verified that instrumental drift was not the cause of sample variation. Indium was selected based on its minimal occurrence in marine samples and low polyatomic interference with seawater. Samples were analysed using an X Series II ICP-MS (Thermo Fisher Scientific Inc., Waltham, MA, USA) with PlasmaLab software (Thermo Fisher Scientific Inc., Waltham, MA, USA).

Mussel sectioning and electron microscopy analysis

To probe the spatial location of the labelled MWCNTs with respect to the mussel DG, samples of whole tissues and cross-sections were analysed by environmental scanning electron microscopy (ESEM) and scanning transmission electron microscopy (STEM), respectively. In either case, after the exposure experiments detailed above, a small piece (~5 mm^2) was dissected out of the centre of the digestive gland and fixed in 2% paraformaldehyde, 2.5% glutaraldehyde, 2.5% NaCl, 2 mM $CaCl_2$ in 0.1 M PIPES, pH 7.2 for 3 h. The tissue was then stored in 2.3 M sucrose (in 0.1 M PIPES) until analysis. Two mussels were analysed per treatment. Whole tissue samples were washed with deionised water (four times), transferred onto aluminium specimen stubs and imaged at 3°C (cooled using the Peltier stage) in ESEM mode with the backscatter detector using the FEI Quanta 650 ESEM. Electron transparent sections for STEM analysis were prepared by cutting ~1 mm^2 pieces from the washed whole tissues and sectioning to a thickness of ~180-200 nm at –80°C using the RMC Products PowerTome with the CR-X cryochamber. The cross-sections were transferred onto copper-grid mounted graphene oxide films using the Tokuyasu technique and imaged in dark field STEM using the JOEL 2100+ microscope operating at 200 keV.

Statistical analyses

Statistical tests were conducted using R software. Normality was checked using Lilliefor's test and variance homogeneity was evaluated using Bartlett's test. When necessary, raw data were mathematically transformed (Ln) to achieve normality before proceeding with an ANOVA. When significant, a posteriori Tukey test was performed.

Analysis of interactions

The non-parametric Mann-Whitney *U*-test was used to compare the data from treated mussels with those of the controls (Sforzini *et al.* 2018a). Further analysis of the combined effects of MWCNTs and BaP on DNA Damage (based on Comet Assay) was performed by calculating the Interaction Factor (IF) in order to test for evidence of additivity, synergism and antagonism (Schlesinger *et al.* 1992, Katsifis *et al.* 1996, David *et al.* 2016; Zhang *et al*. 2019):

$$IF = (G_{(MWCNT + BaP)} - C) - [(G_{(MWCNT)} - C) + (G_{(BaP)} - C)]$$

$$= G_{(MWCNT + BaP)} - G_{(MWCNT)} - G_{(BaP)} + C \quad \text{(Equation 1)}$$

$$SEM_{(IF)} = \sqrt{(SEM^2_{(MWCNT + BaP)} + SEM^2_{(MWCNT)} + SEM^2_{(BaP)} + SEM^2_{(C)}]} \quad \text{(Equation 2)}$$

Where IF is the interaction factor: negative IF denotes antagonism, positive IF denotes synergism, and zero IF denotes additivity. G is the mean cell pathological reaction to toxicants (BaP, MWCNTs and BaP + MWCNTs), C is the mean cellular response under control conditions. SEM(x) is the standard error of the mean for group X. Results were expressed as IF, and the 95% confidence limits were derived from the SEM values.

In order to test the mixture IF values against predicted additive values (assumed to have an IF = 0), the predicted additive mean values (A) were calculated:

$$A = (G_{(MWCNT)} - C) + (G_{(BaP)} - C) \quad \text{(Equation 3)}$$

The Pythagorean theorem method for combining standard errors was used to derive combined standard errors for the predicted mean additive values (A) of MWCNTs and BaP (http://mathbench.org.au/statistical-tests/testing-differences-with-the-t-test/6-combining-sds-for-fun-and-profit/). The standard errors for the three C60 and BaP treatments (predicted additive) were derived using the following equation:

$$SEM_{(add)} = \sqrt{(SEM^2_{(MWCNT)} + SEM^2_{(BaP)} + SEM^2_{(C)})} \quad \text{(Equation 4)}$$

This enabled the 95% confidence limits to be derived for the predicted additive values. The confidence limits were used to test the predicted additive values having an IF = 0 against the IF values for the mixtures.

Results

Preparation and characterisation of MWCNTs in seawater

Light scattering and electron microscopy analyses of MWCNTs, shortened and purified by the site-selective, silver-catalysed nanotube oxidation procedure developed previously (Miners *et al.* 2014) which yielded nanotubes ~600 nm in length (Figure 1b), in mussel-exposed seawater indicated the formation of micron-sized aggregates (Figure 1c; S1 and S2). The mean aggregate size determined by DLS (1541±193 nm) showed minimal variation relative to those measured in seawater in the absence

of mussels (1666±198 nm) and in the presence of BaP in mussel-exposed seawater (1642±431 nm).

[Figure 1]

Genotoxicity of MWCNTs in gill and digestive gland cells

At the end of the exposure period, a subtle increase in DNA strand breaks was observed in both the gills and the DG of mussels exposed to the highest concentrations of MWCNTs (0.1 and 1 mg L^{-1}) relative to the seawater-only control (Figure 2). No effect was noted at the lowest concentration (0.01 mg L^{-1}). Furthermore, no increase in micronuclei was observed after MWCNTs exposure in the gills and DG

[Figures 2 and 3]

Co-exposure to BaP and MWCNTs

BaP seawater concentration and uptake in mussel DG

At one hour after dosing, the BaP concentrations in seawater were very close to the nominal concentrations of 64, 81 and 129% for the 5, 50 and 100 µg L^{-1} BaP-only exposures and 48, 78 and 113% for the co-exposures to MWCNT + BaP 5, 50 and 100 µg L^{-1}, respectively. At the end of the exposure, a strong decrease was observed to approximately 95 and 85% of the initial value for exposure to BaP alone and the co-exposure, respectively (Table S1).

As expected, the concentration of BaP in DG in the solvent and MWCNT-only control treatments was below the limit of detection and found to increase with concentration in both the single and co-exposure experiments. However, BaP uptake was significantly lower in mussels co-exposed to MWCNTs and BaP ($p<0.05$), with a 78 and 44% decrease in the uptake for mussels exposed to MWCNTs and BaP at concentrations of 50 and 100 µg L^{-1}, respectively, compared to mussels exposed to BaP alone at the same concentrations (Table 1).

[Table 1 near here]

DNA metabolism gene expression

The transcriptomic approach performed in this work is based on a new platform developed by our group to investigate gene expression profiling of *Mytilus sp.* to environmental stressors. DNA metabolism was the main investigated process over the 15 processes present on the array. Our data revealed that over the 36 targets present on the array covering the DNA metabolism process, 27 were involved in the response to BaP and MWCNTs in DG and 24 in the gills, in at least one condition. In DG, the number of differentially expressed genes (DEGs) involved in the stress response was maximal at 5 µg L^{-1} BaP and 100 µg L^{-1} BaP with 14 DEGs and 12 DEGs respectively (Table 2). However, in the gills the highest number of DEGs was observed in mussels exposed to BaP at 5 µg L^{-1} and 100 µg L^{-1} in the presence of nanotubes (14 DEGs) providing the first clues about the distinct response to stress in the two organs. The heat map clearly showed distinct pattern of DEGs in both tissues (Figures 4, Additional information in Tables S3 and S4). In particular, p53, caspase 3, p63/73 and alkaline phosphatase

targets were found to be the most present in all conditions in the DG and gill tissues showing a distinct pattern between conditions. Indeed, while, the maximum p53 expression level in digestive gland (M value 1.88) was observed in mussels exposed to 5 µg L^{-1} BaP, it was maximum in gills (M value 2.21) for mussels exposed to nanotubes alone. Moreover, caspase 3 gene expression was maintained down regulated in digestive gland tissues exposed to 5 µg L^{-1} BaP (Mvalue -2.30) and nanotubes (M value -3.08). However, the same target was observed to reach a maximum up-regulated level in digestive gland tissues for mussels exposed to MWCNTs and BaP at concentrations of 50-100 µg L^{-1} (M value 2.29). A similar trend was observed in gills. Gene expression analysis by qPCR of selected targets (e.g. p53, caspase3, DNA ligase and topoisomerase) in the same tissues were in trend with the array data (Figure S4).

[Table 2 and Figure 4]

DNA damage in gills and digestive gland after co-exposure

Regarding the comet assay, a tissue-specific response was observed, the DG being more prone to DNA damage compared to the gills. In DG, BaP-induced genotoxicity was concentration-dependent whereas BaP+MWCNTs co-exposure reduced the genotoxic effects. As observed in the previous experiment, exposure to MWCNTs induced DNA strand breaks. In the gills, BaP was only genotoxic at the highest concentration 100 µg L^{-1}, and the co-exposure induced DNA damage only at the intermediate concentration (Figure 5). No significant effect was observed in mussels exposed to MWCNT only. No bulky BaP-DNA adducts (i.e. dG-N^2-BPDE) were detected in any tissue at any of the treatment condition (data not shown).

[Figure 5]

Interactions. Interactions between MWCNTs and BaP on DNA damage are shown in Table 3. There was evidence of an antagonistic interaction between MWCNTs and BaP for DNA damage (Comet assay) at the 5 and 100 µg L^{-1} BaP + MWCNT combination treatment (Table 3).

Analysis of MWCNT uptake in mussels

The presence of gold in the mussel tissues (from the DG, gills and all other tissues pooled together), as diagnostic of the uptake of labelled MWCNTs, was quantified using ICP-MS. The highest amount of gold was found in DG with a mean concentration of 66.73 µg g^{-1} determined, approximately one order of magnitude higher than that observed in the gills (9.42 µg g^{-1}) and all other tissues (5.52 µg g^{-1}). No significant difference was observed in gold level between the different treatments (with or without BaP) in all of the tissues (Figure 6). However, despite an exhaustive electron microscopy investigation of whole and cross-sectioned DG tissues, no direct visualisation of nanotubes was afforded (Figures S5-8).

[Figure 6]

Discussion

Characterisation of MWCNTs in relevant environmental media

The size, shape and surface chemistry of nanoscale materials is known to affect their dispersion in environmental media (Gottschalk *et al.*, 2013). Effective understanding of these physicochemical parameters is key to their potential uptake and consequent biological impact on the marine biota. For carbon-based nanoparticles, such as MWCNTs, this is particularly critical as their surfaces are inherently hydrophobic. MWCNTs therefore have a strong tendency to form aggregates in water, the size and stability of which depends on the properties of both the nanotube and the specific aqueous environment. Indeed, our light scattering measurements (Figure S1) confirm the formation of stable micron-sized agglomerates of nanotubes in mussel-exposed seawater, consistent with analogous studies of MWCNT aggregates in both natural (Anisimova *et al.* 2015) and synthetic seawaters (Xu *et al.* 2011, Cerrillo *et al.* 2015). Interestingly, there was no significant difference in the mean MWCNT aggregate size observed in the mussel-exposed seawater, relative to nanotube aggregates formed in seawater in the absence of mussels or mussel-exposed seawater in the presence of BaP. This suggests that enhancing the propensity for interactions of MWCNTs with either the proteins secreted by mussels or small aromatic molecules does not, in these instances, aid the solvation of individual MWCNTs or affect the observed aggregate sizes formed in seawater. This is however not expected to be a general phenomenon. We therefore recommend that all future ecotoxicological studies on ENPs and NMs feature analysis in the species of interest to account for any possible effects of this nature.

Genotoxicity of MWCNTs

Despite their environmental relevance, little information is available regarding the genotoxicity of carbon nanoparticles and in particular carbon nanotubes in marine invertebrates. In our study, DNA strand breaks were observed in mussel gills and DG after 7-days exposure to 0.10 and 1 mg L^{-1} to MWCNTs and in DG after 3-days exposure to 1 mg L^{-1} MWCNTs. However, no effect was observed in gills after 3-days exposure to 1 mg L^{-1} MWCNTs suggesting a tissue specific genotoxic effect of MWCNTs in mussels. In the marine polychaete *Arenicola marina*, no significant effect on DNA strand breaks was observed after 10 days of exposure to single-walled carbon nanotubes (SWCNTs) through natural sediment (0.003 and 0.03 g/kg) (Galloway *et al.* 2010). Regarding other carbon nanomaterials, increased DNA strand break formation was observed in haemocytes of the marine mussels after exposure to C_{60} at 0.10 and 1 mg L^{-1} for 3 days (Al-Subiai *et al.* 2012, Di *et al.* 2017).

The mechanism of genotoxicity of CNTs in bivalve cells remains unknown. Genotoxic responses of CNTs may arise via direct mechanical injury or as a secondary result of CNT-mediated reactive oxygen species (ROS) generation and therefore oxidative stress (Hutchison *et al.* 2010). Among these mechanisms, oxidative stress is indicated as the key factor of genotoxicity induced by ENMs in bivalve species and their accumulation associated with exposure time is also an important factor in induced-genotoxicity (Rocha *et al.* 2015). Studies by De Marchi *et al.* (2017a, 2017b) in two polychaete species (*Diopatra neapolitana* and *Hediste diversicolor*) and in a marine bivalve (*Ruditapes philippinarum*) showed the induction of oxidative stress after 28 days of exposure to MWCNTs (0.10 and 1.00 mg L^{-1}). Elevated ROS levels may activate cellular stress-dependent signalling pathways. It can directly damage mitochondria, cause DNA fragmentation in the nucleus, cell cycle arrest, apoptosis, and/or inflammatory responses (Nel *et al.* 2006, Maurer-Jones *et al.* 2013). In mammalian cells, it has been

shown that CNTs are able to induce a range of different genotoxic effects. Among these damages, CNTs can also impair the functionality of the mitotic apparatus inducing micronuclei and chromosomal aberrations (VanBerlo *et al.* 2012). However, in our study, no potential aneugenic effect was studied with the micronucleus assay due to lack of species specific centromeric probes. Currently, the genotoxic potential of CNTs in marine invertebrates is not clear. Various factors could influence this phenomenon including differences in experimental design among studies, experimental models used, exposure routes, type of CNTs examined and their preparation procedures, concentrations used and assessed endpoints.

Co-exposure to BaP and MWCNTs

The main objective of this study was to determine if a 'Trojan Horse' effect could be observed when mussels were exposed to MWCNTs in combination with BaP. Mussels accumulated BaP in gills and DG in a manner consistent with previous studies (Canova *et al.* 1998, Banni *et al.* 2017). It was however interesting to observe a decrease in BaP uptake when mussels were co-exposed to MWCNTs. In the Japanese Medaka (*Oryzias latipes*), it has been shown that the coexistence of SWCNTs facilitated the accumulation of phenanthrene in the digestive track of fish and therefore enhanced the whole-body phenanthrene concentration (Su *et al.* 2013). In the earthworm (*Eisenia foetida*), the addition of nanotubes in soil significantly decreased pyrene uptake (Petersen *et al.* 2009b). The same contradictory results were observed with other carbon nanoparticles as for example fullerenes. Della Torre *et al.* (2017) demonstrated that carbon nanopowder facilitated BaP uptake by zebrafish embryos and also affected the distribution of the pollutant in the organism. However, in the same species(i.e. zebrafish larvae), it has been shown that bioavailability of 17α-ethynylestradiol (EE2) was reduced with increasing concentration of nC60 nanoparticles (Park *et al.* 2011). Interestingly, in the digestive gland of *M. galloprovincialis*, comparable BaP tissue concentrations in the presence or absence of C_{60} were observed indicating that, despite the expected strong sorption of BaP on C_{60}, no 'Trojan horse' effect was observed and C_{60}-sorbed B[a]P also remained bioavailable (Barranger *et al.* 2019). In our study, this decrease in BaP uptake when mussels were co-exposed to MWCNTs could be due to high adsorption properties of MWCNTs towards organic compounds and in our case BaP, as widely described for carbon-based ENPs (Yang *et al.* 2006; Hu *et al.* 2008, 2014). Our results showed that BaP is more present in the seawater and less in the DG at the end of the exposure period when MWCNTs are present. Our results suggest that adsorption of BaP on MWCNTs through van der Waals interactions (Figure 1a) in seawater prevent BaP from reaching the mussel. Genotoxic effects measured by the Comet assay confirmed these results showing less DNA damage (i.e, antagonistic interaction, Table 3) in DG when mussels are co-exposed to BaP and MWCNTs, as a result of a lower bioavaibility of BaP adsorbed on MWCNTs (Zhang *et al*. 2019). Previous studies demonstrated that hydrophobic interactions largely drive adsorption of PAHs to MWCNTs (Linard *et al.* 2017). Bioavailability appears to be more influenced by the ability of PAH molecules to access the available adsorption sites, as a function of molecular size and morphology, rather than the type of carbon nanomaterial (Xia *et al.* 2012, Linard *et al.* 2017).

MWCNTs are relatively large supra-molecular structures but may have limited access into the DG cells by endocytosis (Maruyama *et al.* 2015). However, BaP will probably enter the DG cells through a combination of direct transfer (Plant *et al.* 1985) and through endocytosis in bound form mediated by Van der Waals interaction with food proteins and lipids; or else bound to cell surface proteins (Rashid *et al.* 1991, Moore *et al.* 2004, Sayes *et al.* 2004). Most of the observed DNA damage will probably result from oxidative injury to DNA by ROS generated from futile cycling of BaP; as well as being

produced by the MWCNTs and by intra-lysosomal lipofuscin associated with iron (Brunk and Terman 2002, Zangar *et al.* 2004, Moore *et al.* 2007, Sforzini, Moore, *et al.* 2018). The antagonistic interaction observed for highest test concentration of MWCNT + BaP combinations probably result from the consequences of an intracellular limitation of oxidative damage in the mixture treatment (DellaTorre *et al.* 2018). Such limitation may be caused by binding of BaP to externalised non-endocytosed MWCNTs resulting in reduced entry and bioavailability of BaP as evidenced by reduced BaP in DG (Table 1), hence, reducing ROS generation.

In addition to this adsorption effect, according to the literature, various nanoparticles suspended in seawater form aggregates of nano- and microsizes (Canesi *et al.* 2010a, Canesi *et al.* 2010b, Canesi *et al.* 2014). In the presence of bivalves, the aggregates associate with mucus are suggested to be deposited along the byssus thread and settle on the bottom of the aquarium (Canesi *et al.* 2010b). Thus, the amount of nanoparticles, and in our case of BaP adsorbed on it, captured by mollusks is significantly less than that expected on the basis of the initial concentration of the suspension. These results could lead to the hypothesis that the high sedimentation rate observed within aquarium highlighted that MWCNTs would transport PAHs mainly in sediments (DellaTorre *et al.* 2017, 2018).

Regarding other genotoxic effects, in our study no bulky BaP-DNA adducts were detected in any of the treatments. This result differs with a previous experiment (Banni *et al*. 2017), where bulky DNA adducts (i.e. dG-N^2-BDDE) were detected after exposure to BaP using the same experimental design (same concentrations and exposure duration). One explanation could be the physiological state of the mussels. It is known that mussels from the species *Mytilus galloprovincialis*, are spawning all year around compared to *Mytilus edulis* which has a specific period of spawning in May and October. Even if we performed our experiment in November, gonads of mussels were mature, and it is known that during maturation there is a drop in the biotransformation process that could explain the lack of bulky BaP-DNA adducts in DG (Solé *et al.* 1995, Shaw *et al.* 2004).

In addition to the biomarkers of genotoxic effects, the transcriptomics data provided interesting information regarding the expression of genes involved in DNA metabolism. We noticed a marked regulation of genes involved in DNA metabolism in both tissues in mussels exposed to BaP alone or in combination with MWCNTs. However, exposure to MWCNTs alone resulted in a very low number of DEGs in both tissues. Interestingly, mussels exposed to the mixtures of BaP and nanotubes manifested a significant increase in the number of DEGs in gills while no marked increase was observed in DG. In the last decade, transcriptomics has proved to be a reliable tool, increasing our understanding of many important physiological processes in marine organisms in response to environmental stressors such as chemicals (Negri *et al.* 2013; Sforzini *et al.* 2018b) as well as to physiological parameters such as annual cycle (Banni *et al.* 2011). Moreover, transcriptional control can allow stressed organisms to cope with the alteration of cellular functions and to avoid cellular damage.

A significant alteration was recorded by the Comet assay in DG cells from animals exposed to BaP alone, and co-exposed to BaP and MWCNTs but to lesser extent. Transcriptomic data corroborated these results showing less DEGs in DG of mussels co-exposed to the mixture. In gills however mussels exposed to the mixture of BaP and MWCNTs exhibited a significant increase in the number of DEGs. These results are not correlated with the genotoxic response measured by Comet assay showing no additional effect when mussels are co-exposed to both contaminants. The relatively short exposure period (3 days) may explain the absence of cellular alterations where gene expression occurs.

The investigation of DNA damage response genes coding for caspase (HQ424451.1) revealed a marked

up-regulation of apoptotic genes in gills of mussels exposed to the highest BaP concentration alone or in combination with nanotubes. DNA repair-related enzymes (DNA ligase: AJ624686.1; p53: KC545827.1) were however markedly up-regulated in animals exposed to lower BaP concentration and to nanotubes (data confirmed by qPCR). Mussel's cells may react to DNA alterations via p53-mediated cell cycle arrest or apoptosis, upon high or irreparable DNA damage, p53 promotes the cells towards apoptosis (Schwartz and Rotter 1998).

Overall, these results highlight that, once inside the organism, BaP and MWCNTs activate genes involved in DNA metabolism in a different way to the activation by BaP or MWCNTs alone. Genotoxic and transcriptomic data may suggest a tissue-specific response and the occurrence of a DNA repair or apoptosis events with respect to the applied BaP/nanotubes concentrations. In our case, it is difficult to conclude the exact mechanisms of this response. Despite the fact that less BaP is uptaken when mussels are co-exposed, gills displayed higher DEGs in the co-exposure treatment, which is not the case for DG. It has been shown that BaP accumulates differently in tissue when zebrafish embryos are co-exposed to carbon nanopowder (CNPW) and BaP (Della Torre *et al.* 2017). In our study, only one tissue (i.e. DG) has been analysed for BaP uptake making it difficult to a make a conclusion.

Tracking MWCNTs in the mussel DG

One of the most significant challenges when probing the uptake of nanoscale materials, including carbon nanotubes, in marine biota is developing reliable and quantitative methods for their detection. In this respect, CNTs represent a particular problem as their inherent structural polydispersity (i.e. broad range of diameters and lengths) hinders conventional analytical approaches, such as chromatographic separation. Moreover, methods based on elemental analysis and spectroscopic techniques are generally not feasible because of the presence of organic matter. Spectrofluorometric analysis is one approach that has been used successfully to quantify nanotubes in mouse cells and rabbits (Cherukuri *et al.* 2004, 2006). However, as this technique is only applicable to semiconducting SWCNTs. Insensitive to either individual metallic SWCNTs or bundles containing metallic SWCNTs, the electronic properties and aggregation characteristics of nanotubes in environmental systems is often unknown. This approach has therefore limited potential (O'Connell *et al.* 2002). Raman spectroscopy was used to detect SWCNTs qualitatively in the aquatic organism *D. magna* (Roberts *et al.* 2007); yet, this approach cannot provide quantitative results and is best suited for SWCNTs owing to the effects of resonant signal enhancement. A method used recently to detect carbon nanotubes in biological systems is tagging them with molecules that are either bonded to radioactive isotopes or are themselves fluorescent (Kam *et al.* 2004, 2006, Singh *et al.* 2006). The use of such probes however depends on the stability of its attachment to the nanotubes and, for radioactive labelling, attachment of the isotope to the polymer. The addition of such bulky tags likely influences the physicochemical properties of the nanotubes and thus their environmental behaviours.

The novel approach explored in our study was the utilisation of gold-labelled MWCNTs to improve the traceability of nanotubes in biological samples. Indeed, ICP-MS results indicated the presence of gold in mussel tissues, particularly in the digestive gland. Thus, bioaccumulation of MWCNTs in mussels at the whole tissue level was confirmed, consistent with analogous previous studies using other aquatic species (Templeton *et al.* 2006, Roberts *et al.* 2007, Smith *et al.* 2007, Ferguson *et al.* 2008, Petersen, Akkanen, *et al.* 2009). In an attempt to probe the spatial location of labelled MWCNTs at the cellular level, we analysed samples using electron microscopy. It is important to note that it has been shown previously that incorrect sample preparation and subsequent image interpretation may lead to the

generation of false positives and inaccurate conclusions (Edgington *et al.* 2014). The most common issue of this nature is that all high-contrast material presented in bright-field images of the sections (where dark features correspond to structures comprising high atomic number elements) are assumed to be from the specific artificial nanomaterial under examination. However, these may, in fact, be related to unknown organic or inorganic matter or artefacts induced during the staining preparation that is standard protocol for producing high quality transmission electron microscopy images. It is for this reason that we elected to use gold-labelled nanotubes, in the absence of stains, in our studies. This provided a uniquely diagnostic handle enabling us to correlate the presence of any foreign materials with their exact elemental composition. Indeed, our combined electron microscopy and *in situ* spectroscopy approach enabled us to show the presence of numerous metals in nanoparticle form in both ESEM images of the whole tissues and STEM images of the digestive gland cross-sections from control samples in the absence of labelled MWCNTs (Figures S5 and S7). Yet, despite an extensive electron microscopy examination we were not able to visualise AuNP@MWCNTs in any of the samples appraised (Figures S5 and S7). The absence of evidence from STEM/EDX analysis of the cross-section is not unexpected given the large dimensions of the mussel (~5 mm^2) relative to the size of the sections (~180-200 nm in thickness). The fact that no evidence was observed in images of the whole tissue and that gold is detected from bulk ICP-MS analysis means that MWCNTs must be located within the internal structures of the DG. It suggests that the local probe nature of STEM confers a sampling issue, though visualisation of their location at the cellular level remains elusive. These results emphasise the challenge of direct imaging of nanostructures in biological samples and the importance of using a range of different analytical techniques in order to obtain a good understanding of these complex systems.

It should be noted that in our experiment the results were obtained at concentrations well above environmentally realistic concentrations, especially for MWCNTs. As stated earlier, the predicted environmental concentration for CNTs is at low ng/L. In a review, the assembled results from different experiments indicate that carbon nanomaterials (CNMs) are not expected to be toxic to aquatic organisms at environmentally relevant concentrations (Freixa *et al.* 2018). Toxic effects of CNMs to aquatic organisms occur under high concentrations in short-term experiments (Jackson *et al.* 2013). As stated in the review however (Freixa *et al.* 2018), in the near future numerous commercial products are expected to include nanoparticles in their formulations (DeVolder *et al.* 2013), indicating that, the concentration of CNMs in aquatic systems could increase to which organisms could be chronically exposed. It should also be noted that the antagonistic response observed in the current study between BaP and MWCNTs is based on a single concentration of the carbon nanotubes and as such represents a general overview of potential toxicological behaviour. It is possible that this antagonistic interaction could change when another concentration range is selected. Future studies must include more realistic exposure scenarios to estimate accurately toxicity of nanomaterials.

Conclusion

Our findings highlight that impacts of the co-exposure of organic pollutants and CNTs on the bioavailability and accumulation of the contaminants are mixed and species specific, indicating that in the case of BaP the accumulation of this PAH is not facilitated by the presence of MWCNTs in *M. galloprovincialis.* Environmentally realistic experiments are mandatory in order to identify and explain the possible threat of ENMs to organisms. Many variables can modify the fate and consequently toxic effects of ENPs and adsorbed pollutants. Fine characterisation of nanoparticles in (sea)water (including characterisation of the adsorbed contaminants) and localization are the main challenge to

understand the toxic effect of this emerging contaminant in the environment. Overall, our study demonstrate the challenges for hazard and risk assessments posed by ENMs and contribute to improve our understanding of their potential interactive effects with other ubiquitous pollutants on an ecologically an economically important marine organism.

Acknowledgements

We would like to thank Dr Alessandro La Torre (University of Nottingham) for technical support. The views expressed in this article are those of the authors and not necessarily of the funding agencies including the National Health Service, the National Institute for Health Research, the Department of Health and Social Care or Public Health England.

Disclosure statement

The authors report no conflict of interest.

Funding

This study is mainly supported by Natural Environment Research Council (NERC), UK (Grant No. NE/L006782/1; PI: ANJ). Additional Support from the Engineering and Physical Sciences Research Council (EPSRC) [Grant No. EP/L022494/1] and the University of Nottingham is acknowledged. Work at King's College London was further supported by the National Institute for Health Research Health Protection Research Unit (NIHR HPRU) in Health Impact of Environmental Hazards at King's College London in partnership with Public Health England (PHE) and Imperial College London.

Word Count: 7918 (excluding references)

References

Acevedo-Whitehouse, K., Cole, K.J., Phillips, D.H., Jepson, P.D., Deaville, R., and Arlt, V.M., 2018. Hepatic DNA damage in harbour porpoises (Phocoena phocoena) stranded along the English and Welsh coastlines. *Environmental and Molecular Mutagenesis*, 59 (7), 613–624.

Akcha, F., Burgeot, T., Venier, P., and Narbonne, J.F., 1999. Relationship between kinetics of benzo[a]pyrene bioaccumulation and DNA binding in the mussel Mytilus galloprovincialis. *Bulletin of Environmental Contamination and Toxicology*, 62 (4), 455–462.

Al-Subiai, S.N., Arlt, V.M., Frickers, P.E., Readman, J.W., Stolpe, B., Lead, J.R., Moody, A.J., and Jha, A.N., 2012. Merging nano-genotoxicology with eco-genotoxicology: An integrated approach to determine interactive genotoxic and sub-lethal toxic effects of C 60 fullerenes and fluoranthene in marine mussels, Mytilus sp. *Mutation Research - Genetic Toxicology and Environmental*

632 *Mutagenesis*, 745 (1–2), 92–103.

633 Anisimova, A.A., Chaika, V. V., Kuznetsov, V.L., and Golokhvast, K.S., 2015. Study of the influence of
634 multiwalled carbon nanotubes (12–14 nm) on the main target tissues of the bivalve Modiolus
635 modiolus. *Nanotechnologies in Russia*, 10 (3–4), 278–287.

636 Banni, M., Negri, A., Mignone, F., Boussetta, H., Viarengo, A., and Dondero, F., 2011. Gene
637 expression rhythms in the mussel mytilus galloprovincialis (Lam.) across an annual cycle. *PLoS*
638 *ONE*, 6 (5).

639 Banni, M., Sforzini, S., Arlt, V.M., Barranger, A., Dallas, L.J., Oliveri, C., Aminot, Y., Pacchioni, B.,
640 Millino, C., Lanfranchi, G., Readman, J.W., Moore, M.N., Viarengo, A., and Jha, A.N., 2017.
641 Assessing the impact of Benzo[a]pyrene on Marine Mussels: Application of a novel targeted
642 low density microarray complementing classical biomarker responses. *PLOS ONE*, 12 (6),
643 e0178460.

644 Barranger, A., Langan, L.M., Sharma, V., Rance, G.A., Aminot, Y., Weston, N.J., Akcha, F., Moore,
645 M.N., Arlt, V.M., Khlobystov, A.N., Readman, J.W., and Jha, A.N., 2019. Antagonistic
646 Interactions between Benzo[a]pyrene and Fullerene (C60) in Toxicological Response of Marine
647 Mussels. *Nanomaterials*, 9 (7), 987.

648 Baumard, P., Budzinski, H., and Garrigues, P., 1998. Environmental Chemistry POLYCYCLIC
649 AROMATIC HYDROCARBONS IN SEDIMENTS AND MUSSELS OF THE. *Environmental Toxicology*,
650 17 (5), 765–776.

651 Baumard, P., Budzinski, H., Garrigues, P., Dizer, H., and Hansen, P.D., 1999. Polycyclic aromatic
652 hydrocarbons in recent sediments and mussels (Mytilus edulis) from the Western Baltic Sea:
653 Occurrence, bioavailability and seasonal variations. *Marine Environmental Research*, 47 (1), 17–
654 47.

655 Beigbeder, A., Degee, P., Conlan, S.L., Mutton, R.J., Clare, A.S., Pettitt, M.E., Callow, M.E., Callow, J. a,
656 and Dubois, P., 2008. Preparation and characterisation of silicone-based coatings filled with
657 carbon nanotubes and natural sepiolite and their application as marine fouling-release
658 coatings. *Biofouling*, 24 (4), 291–302.

659 Bjorkland, R., Tobias, D.A., and Petersen, E.J., 2017. Increasing evidence indicates low

660 bioaccumulation of carbon nanotubes. *Environ. Sci.: Nano*, 4 (4), 747–766.

661 Bolognesi, C. and Fenech, M., 2012. Mussel micronucleus cytome assay. *Nature Protocols*, 7 (6),
662 1125–1137.

663 Brunk, U.T. and Terman, A., 2002. Lipofuscin: Mechanisms of age-related accumulation and
664 influence on cell function. *Free Radical Biology and Medicine*, 33 (5), 611–619.

665 Canesi, L., Ciacci, C., and Balbi, T., 2015. Interactive effects of nanoparticles with other contaminants
666 in aquatic organisms: Friend or foe? *Marine Environmental Research*, 111, 128–134.

667 Canesi, L., Ciacci, C., Vallotto, D., Gallo, G., Marcomini, A., and Pojana, G., 2010a. In vitro effects of
668 suspensions of selected nanoparticles (C60 fullerene, TiO2, SiO2) on Mytilus hemocytes.
669 *Aquatic Toxicology*, 96 (2), 151–158.

670 Canesi, L., Fabbri, R., Gallo, G., Vallotto, D., Marcomini, A., and Pojana, G., 2010b. Biomarkers in
671 Mytilus galloprovincialis exposed to suspensions of selected nanoparticles (Nano carbon black,
672 C60 fullerene, Nano-TiO2, Nano-SiO2). *Aquatic Toxicology*, 100 (2), 168–177.

673 Canesi, L., Frenzilli, G., Balbi, T., Bernardeschi, M., Ciacci, C., Corsolini, S., Della Torre, C., Fabbri, R.,
674 Faleri, C., Focardi, S., Guidi, P., Kočan, A., Marcomini, A., Mariottini, M., Nigro, M., Pozo-
675 Gallardo, K., Rocco, L., Scarcelli, V., Smerilli, A., and Corsi, I., 2014. Interactive effects of n-TiO2
676 and 2,3,7,8-TCDD on the marine bivalve Mytilus galloprovincialis. *Aquatic Toxicology*, 153, 53–
677 65.

678 Canova, S., Degan, P., Peters, L.., Livingstone, D.., Voltan, R., and Venier, P., 1998. Tissue dose, DNA
679 adducts, oxidative DNA damage and CYP1A-immunopositive proteins in mussels exposed to
680 waterborne benzo[a]pyrene. *Mutation Research/Fundamental and Molecular Mechanisms of*
681 *Mutagenesis*, 399 (1), 17–30.

682 Cerrillo, C., Barandika, G., Igartua, A., Areitioaurtena, O., Marcaide, A., and Mendoza, G., 2015.
683 Ecotoxicity of multiwalled carbon nanotubes: Standardization of the dispersion methods and
684 concentration measurements. *Environmental Toxicology and Chemistry*, 34 (8), 1854–1862.

685 Cherukuri, P., Bachilo, S.M., Litovsky, S.H., and Weisman, R.B., 2004. Near-Infrared Fluorescence
686 Microscopy of Single-Walled Carbon Nanotubes in Phagocytic Cells. *Journal of the American*
687 *Chemical Society*, 126 (48), 15638–15639.

688 Cherukuri, P., Gannon, C.J., Leeuw, T.K., Schmidt, H.K., Smalley, R.E., Curley, S.A., and Weisman, R.B.,
689 2006. Mammalian pharmacokinetics of carbon nanotubes using intrinsic near-infrared
690 fluorescence. *Proceedings of the National Academy of Sciences*, 103 (50), 18882–18886.

691 Cho, K., Wang, X., Nie, S., Chen, Z., and Shin, D.M., 2008. Therapeutic nanoparticles for drug delivery
692 in cancer. *Clinical Cancer Research*, 14 (5), 1310–1316.

693 Conesa, A., Götz, S., García-Gómez, J.M., Terol, J., Talón, M., and Robles, M., 2005. Blast2GO: A
694 universal tool for annotation, visualization and analysis in functional genomics research.
695 *Bioinformatics*, 21 (18), 3674–3676.

696 D'Agata, A., Fasulo, S., Dallas, L.J., Fisher, A.S., Maisano, M., Readman, J.W., and Jha, A.N., 2014.
697 Enhanced toxicity of 'bulk' titanium dioxide compared to 'fresh' and 'aged' nano-TiO2 in marine
698 mussels (Mytilus galloprovincialis). *Nanotoxicology*, 8 (5), 549–58.

699 Dallas, L.J., Bean, T.P., Turner, A., Lyons, B.P., and Jha, A.N., 2013. Oxidative DNA damage may not
700 mediate Ni-induced genotoxicity in marine mussels: assessment of genotoxic biomarkers and
701 transcriptional responses of key stress genes. *Mutation research*, 754 (1–2), 22–31.

702 David, R., Ebbels, T., and Gooderham, N., 2016. Synergistic and Antagonistic Mutation Responses of
703 Human MCL-5 Cells to Mixtures of Benzo[a]pyrene and 2-Amino-1-Methyl-6-
704 Phenylimidazo[4,5- b]pyridine: Dose-Related Variation in the Joint Effects of Common Dietary
705 Carcinogens. *Environmental Health Perspectives*, 124 (1), 88–96.

706 DellaTorre, C., Maggioni, D., Ghilardi, A., Parolini, M., Santo, N., Landi, C., Madaschi, L., Magni, S.,
707 Tasselli, S., Ascagni, M., Bini, L., La Porta, C., Del Giacco, L., and Binelli, A., 2018. The
708 interactions of fullerene C60 and Benzo(A)pyrene influence their bioavailability and toxicity to
709 zebrafish embryos. *Environmental Pollution*, 241, 999–1008.

710 DellaTorre, C., Parolini, M., Del Giacco, L., Ghilardi, A., Ascagni, M., Santo, N., Maggioni, D., Magni, S.,
711 Madaschi, L., Prosperi, L., La Porta, C., and Binelli, A., 2017. Adsorption of B(α)P on carbon
712 nanopowder affects accumulation and toxicity in zebrafish (Danio rerio) embryos.
713 *Environmental Science: Nano*, 4 (5).

714 DeMarchi, L., Neto, V., Pretti, C., Figueira, E., Chiellini, F., Soares, A.M.V.M., and Freitas, R., 2017a.
715 Physiological and biochemical responses of two keystone polychaete species: Diopatra

716 neapolitana and Hediste diversicolor to Multi-walled carbon nanotubes. *Environmental*
717 *Research*, 154 (December 2016), 126–138.

718 DeMarchi, L., Neto, V., Pretti, C., Figueira, E., Chiellini, F., Soares, A.M.V.M., and Freitas, R., 2017b.
719 The impacts of emergent pollutants on Ruditapes philippinarum: biochemical responses to
720 carbon nanoparticles exposure. *Aquatic Toxicology*, 187, 38–47.

721 DeVolder, M.F.L., Tawfick, S.H., Baughman, R.H., and Hart, J.A., 2013. Carbon nanotubes: present
722 and future commercial applications. *Science.*, 339 (February), 535–539.

723 Di, Y., Aminot, Y., Schroeder, D.C., Readman, J.W., and Jha, A.N., 2016. Integrated biological
724 responses and tissue-specific expression of p53 and ras genes in marine mussels following
725 exposure to benzo(α)pyrene and C60 fullerenes, either alone or in combination. *Mutagenesis*,
726 00, 1–14.

727 Di, Y., Schroeder, D.C., Highfield, A., Readman, J.W., and Jha, A.N., 2011. Tissue-specific expression of
728 p53 and ras genes in response to the environmental genotoxicant benzo(a)pyrene in marine
729 mussels. *Environmental Science and Technology*, 45 (20), 8974–8981.

730 Edgington, A.J., Petersen, E.J., Herzing, A.A., Podila, R., Rao, A., and Klaine, S.J., 2014. Microscopic
731 investigation of single-wall carbon nanotube uptake by *Daphnia magna*. *Nanotoxicology*, 8
732 (sup1), 2–10.

733 Ferguson, P.L., Chandler, G.T., Templeton, R.C., Demarco, A., Scrivens, W.A., and Englehart, B.A.,
734 2008. Influence of sediment - Amendment with single-walled carbon nanotubes and diesel soot
735 on bioaccumulation of hydrophobic organic contaminants by benthic invertebrates.
736 *Environmental Science and Technology*, 42 (10), 3879–3885.

737 Foss Hansen, S., Heggelund, L.R., Revilla Besora, P., Mackevica, A., Boldrin, A., and Baun, A., 2016.
738 Nanoproducts - What is actually available to European consumers? *Environmental Science:*
739 *Nano*, 3 (1), 169–180.

740 Freixa, A., Acuña, V., Sanchís, J., Farré, M., Barceló, D., and Sabater, S., 2018. Ecotoxicological effects
741 of carbon based nanomaterials in aquatic organisms. *Science of The Total Environment*, 619–
742 620, 328–337.

743 Galloway, T., Lewis, C., Dolciotti, I., Johnston, B.D., Moger, J., and Regoli, F., 2010. Sublethal toxicity

744 of nano-titanium dioxide and carbon nanotubes in a sediment dwelling marine polychaete.
745 *Environmental Pollution*, 158 (5), 1748–1755.

746 Giese, B., Klaessig, F., Park, B., Kaegi, R., Steinfeldt, M., Wigger, H., Von Gleich, A., Gottschalk, F.,
747 2018. Risks, release and concentrations of engineered nanomaterials in the environment.
748 *Scientific Reports* 8: 1565.

749 Goldberg, E.D., 1987. Heavy metal analyses in the marine environment - approaches to quality
750 control. *Marine Chemistry*, 22 (2–4), 117–124.

751 Gomes, T., Araújo, O., Pereira, R., Almeida, A.C., Cravo, A., and Bebianno, M.J., 2013. Genotoxicity of
752 copper oxide and silver nanoparticles in the mussel Mytilus galloprovincialis. *Marine*
753 *Environmental Research*, 84, 51–59.

754 Gottschalk, F., Sun, T., and Nowack, B., 2013. Environmental concentrations of engineered
755 nanomaterials: Review of modeling and analytical studies. *Environmental Pollution*, 181, 287–
756 300.

757 Halldórsson, H.P., De Pirro, M., Romano, C., Svavarsson, J., and Sarà, G., 2008. Immediate biomarker
758 responses to benzo[a]pyrene in polluted and unpolluted populations of the blue mussel
759 (Mytilus edulis L.) at high-latitudes. *Environment International*, 34 (4), 483–489.

760 Hu, X., Li, J., Chen, Q., Lin, Z., and Yin, D., 2014. Combined effects of aqueous suspensions of
761 fullerene and humic acid on the availability of polycyclic aromatic hydrocarbons: Evaluated
762 with negligible depletion solid-phase microextraction. *Science of The Total Environment*, 493,
763 12–21.

764 Hu, X., Liu, J., Mayer, P., and Jiang, G., 2008. Impacts of some environmentally relevant parameters
765 on the sorption of polycyclic aromatic hydrocarbons to aqueous suspensions of fullerene.
766 *Environmental Toxicology and Chemistry*, 27 (9), 1868.

767 Hutchison, G.R., Christensen, F.M., Aschberger, K., Johnston, H.J., Hankin, S., Stone, V., and Peters,
768 S., 2010. A critical review of the biological mechanisms underlying the in vivo and in vitro
769 toxicity of carbon nanotubes: The contribution of physico-chemical characteristics .
770 *Nanotoxicology*, 4 (2), 207–246.

771 Jackson, P., Jacobsen, N.R., Baun, A., Birkedal, R., Kühnel, D., Jensen, K.A., Vogel, U., and Wallin, H.,

772 2013. Bioaccumulation and ecotoxicity of carbon nanotubes. *Chemistry Central Journal*, 7 (1),
773 154.

774 Kam, N.W.S., Jessop, T.C., Wender, P.A., and Dai, H., 2004. Nanotube molecular transporters:
775 Internalization of carbon nanotube-protein conjugates into mammalian cells. *Journal of the*
776 *American Chemical Society*, 126 (22), 6850–6851.

777 Kam, N.W.S., Liu, Z., and Dai, H., 2006. Carbon nanotubes as intracellular transporters for proteins
778 and DNA: An investigation of the uptake mechanism and pathway. *Angewandte Chemie -*
779 *International Edition*, 45 (4), 577–581.

780 Katsifis, S.P., Kinney, P.L., Hosselet, S., Burns, F.J., and Christie, N.T., 1996. Interaction of nickel with
781 mutagens in the induction of sister chromatid exchanges in human lymphocytes. *Mutation*
782 *Research/Environmental Mutagenesis and Related Subjects*, 359 (1), 7–15.

783 LaTorre, A., Rance, G. a., El Harfi, J., Li, J., Irvine, D.J., Brown, P.D., and Khlobystov, A.N., 2010.
784 Transport and encapsulation of gold nanoparticles in carbon nanotubes. *Nanoscale*, 2, 1006–
785 1010.

786 Linard, E.N., Apul, O.G., Karanfil, T., Van Den Hurk, P., and Klaine, S.J., 2017. Bioavailability of Carbon
787 Nanomaterial-Adsorbed Polycyclic Aromatic Hydrocarbons to Pimphales promelas: Influence of
788 Adsorbate Molecular Size and Configuration. *Environmental Science and Technology*, 51 (16),
789 9288–9296.

790 Livingstone, D.R. and Pipe, R.K., 1992. Mussels and environmental contaminants: molecular and
791 cellular aspects. *Dev. Aquac. Fish. Sci*, 25, 424–464.

792 Maruyama, K., Haniu, H., Saito, N., Matsuda, Y., Tsukahara, T., Kobayashi, S., Tanaka, M., Aoki, K.,
793 Takanashi, S., Okamoto, M., and Kato, H., 2015. Endocytosis of multiwalled carbon nanotubes
794 in bronchial epithelial and mesothelial cells. *BioMed Research International*, 2015.

795 Maurer-Jones, M.A., Gunsolus, I.L., Murphy, C.J., and Haynes, C.L., 2013. Toxicity of engineered
796 nanoparticles in the environment. *Analytical Chemistry*, 85 (6), 3036–3049.

797 Miners, S.A., Rance, G.A., and Khlobystov, A.N., 2016. Chemical reactions confined within carbon
798 nanotubes. *Chemical Society Reviews*, 45 (17), 4727–4746.

Miners, S.A., Rance, G.A., La Torre, A., Kenny, S.M., and Khlobystov, A.N., 2014. Controlled oxidative cutting of carbon nanotubes catalysed by silver nanoparticles. *Journal of Materials Chemistry C*, 2 (39), 8357–8363.

Moore, M.N., Depledge, M.H., Readman, J.W., and Paul Leonard, D.R., 2004. An integrated biomarker-based strategy for ecotoxicological evaluation of risk in environmental management. *Mutation Research - Fundamental and Molecular Mechanisms of Mutagenesis*, 552 (1–2), 247–268.

Moore, M.N., Viarengo, A., Donkin, P., and Hawkins, A.J.S., 2007. Autophagic and lysosomal reactions to stress in the hepatopancreas of blue mussels. *Aquatic Toxicology*, 84 (1), 80–91.

Moore, M.N., Wedderburn, J., Clarke, K.R., McFadzen, I., Lowe, D.M., Readman, J.W. 2018. Emergent synergistic lysosomal toxicity of chemical mixtures in molluscan blood cells (hemocytes). *Environmental Pollut*ion, 235, 1006-1014.

Negri, A., Oliveri, C., Sforzini, S., Mignione, F., Viarengo, A., and Banni, M., 2013. Transcriptional Response of the Mussel Mytilus galloprovincialis (Lam.) following Exposure to Heat Stress and Copper. *PLoS ONE*, 8 (6).

Nel, A., Xia, T., Mädler, L., and Li, N., 2006. Toxic potential of materials at the nanolevel. *Science*.

Nikolaou, A., Kostopoulou, M., Petsas, A., Vagi, M., Lofrano, G., and Meric, S., 2009. Levels and toxicity of polycyclic aromatic hydrocarbons in marine sediments. *TrAC - Trends in Analytical Chemistry*, 28 (6), 653–664.

O'Connell, M.J., Bachilo, S.M., Huffman, C.B., Moore, V.C., Strano, M.S., Haroz, E.H., Rialon, K.L., Boul, P.J., Noon, W.H., Kittrell, C., Ma, J., Hauge, R.H., Weisman, R.B., and Smalley, R.E., 2002. Band Gap Fluorescence from Individual Single-Walled Carbon Nanotubes. *Science*, 297 (5581), 593 LP – 596.

Park, J.-W., Henry, T.B., Ard, S., Menn, F.-M., Compton, R.N., and Sayler, G.S., 2011. The association between nC(60) and 17α-ethinylestradiol (EE2) decreases EE2 bioavailability in zebrafish and alters nanoaggregate characteristics. *Nanotoxicology*, 5 (September), 406–416.

Petersen, E.J., Akkanen, J., Kukkonen, J.V.K., and Weber, W.J., 2009a. Biological uptake and depuration of carbon nanotubes by daphnia magna. *Environmental Science and Technology*, 43

827 (8), 2969–2975.

828 Petersen, E.J., Pinto, R.A., Landrum, P.F., and Weber, W.J., 2009b. Influence of Carbon Nanotubes on
829 Pyrene Bioaccumulation from Contaminated Soils by Earthworms. *Environmental Science &*
830 *Technology*, 43 (11), 4181–4187.

831 Phillips, D.H. and Arlt, V.M., 2014. 32P-Postlabeling Analysis of DNA Adducts. *In*: P. Keohavong and
832 S.G. Grant, eds. *Molecular Toxicology Protocols*. Totowa, NJ: Humana Press, 127–138.

833 Plant, A.L., Benson, D.M., and Smith, L.C., 1985. Cellular uptake and intracellular localization of
834 benzo(a)pyrene by digital fluorescence imaging microscopy. *Journal of Cell Biology*, 100 (4),
835 1295–1308.

836 Rance, G.A., Marsh, D.H., and Khlobystov, A.N., 2008. Extinction coefficient analysis of small
837 alkanethiolate-stabilised gold nanoparticles. *Chemical Physics Letters*, 460 (1–3), 230–236.

838 Rashid, F., Horobin, R.W., and Williams, M.A., 1991. Predicting the behaviour and selectivity of
839 fluorescent probes for lysosomes and related structures by means of structure-activity models.
840 *The Histochemical Journal*, 23 (10), 450–459.

841 Roberts, A.P., Mount, A.S., Seda, B., Souther, J., Qiao, R., Lin, S., Pu, C.K., Rao, A.M., and Klaine, S.J.,
842 2007. In vivo biomodification of lipid-coated carbon nanotubes by Daphnia magna.
843 *Environmental Science and Technology*, 41 (8), 3028–3029.

844 Rocha, T.L., Gomes, T., Sousa, V.S., Mestre, N.C., and Bebianno, M.J., 2015. Ecotoxicological impact
845 of engineered nanomaterials in bivalve molluscs: An overview. *Marine Environmental Research*,
846 111, 74–88.

847 Sayes, C.M., Fortner, J.D., Guo, W., Lyon, D., Boyd, A.M., Ausman, K.D., Tao, Y.J., Sitharaman, B.,
848 Wilson, L.J., Hughes, J.B., West, J.L., and Colvin, V.L., 2004. The Differential Cytotoxicity of
849 Water-Soluble Fullerenes. *Nano Letters*, 4 (10), 1881–1887.

850 Schlesinger, R.B., Zelikoff, J.T., Chen, L.C., and Kinney, P.L., 1992. Assessment of toxicologic
851 interactions resulting from acute inhalation exposure to sulfuric acid and ozone mixtures.
852 *Toxicology and Applied Pharmacology*, 115 (2), 183–190.

853 Schwartz, D. and Rotter, V., 1998. P53-Dependent Cell Cycle Control: Response To Genotoxic Stress.

854 *Seminars in cancer biology*, 8 (5), 325–336.

855 Sforzini, S., Moore, M.N., Oliveri, C., Volta, A., Jha, A., Banni, M., and Viarengo, A., 2018a. Role of
856 mTOR in autophagic and lysosomal reactions to environmental stressors in molluscs. *Aquatic*
857 *Toxicology*, 195 (December 2017), 114–128.

858 Sforzini, S., Oliveri, C., Orrù, A., Chessa, G., Pacchioni, B., Millino, C., Jha, A.N., Viarengo, A., and
859 Banni, M., 2018b. Application of a new targeted low density microarray and conventional
860 biomarkers to evaluate the health status of marine mussels: A field study in Sardinian coast,
861 Italy. *Science of The Total Environment*, 628–629, 319–328.

862 Shaw, J.P., Large, A.T., Donkin, P., Evans, S. V, Staff, F.J., Livingstone, D.R., Chipman, J.K., and Peters,
863 L.D., 2004. Seasonal variation in cytochrome P450 immunopositive protein levels, lipid
864 peroxidation and genetic toxicity in digestive gland of the mussel Mytilus edulis. *Aquatic*
865 *Toxicology*, 67 (4), 325–336.

866 Singh, R., Pantarotto, D., Lacerda, L., Pastorin, G., Klumpp, C., Prato, M., Bianco, A., and Kostarelos,
867 K., 2006. Tissue biodistribution and blood clearance rates of intravenously administered carbon
868 nanotube radiotracers. *Proceedings of the National Academy of Sciences*, 103 (9), 3357–3362.

869 Smith, C.J., Shaw, B.J., and Handy, R.D., 2007. Toxicity of single walled carbon nanotubes to rainbow
870 trout, (Oncorhynchus mykiss): Respiratory toxicity, organ pathologies, and other physiological
871 effects. *Aquatic Toxicology*, 82 (2), 94–109.

872 Sogbanmu, T.O., Nagy, E., Phillips, D.H., Arlt, V.M., Otitoloju, A.A., and Bury, N.R., 2016. Lagos lagoon
873 sediment organic extracts and polycyclic aromatic hydrocarbons induce embryotoxic,
874 teratogenic and genotoxic effects in Danio rerio (zebrafish) embryos. *Environ Sci Pollut Res Int*.

875 Solé, M., Porte, C., and Albaigés, J., 1995. Seasonal variation in the mixed-function oxygenase system
876 and antioxidant enzymes of the mussel Mytilus galloprovincialis. *Environmental Toxicology and*
877 *Chemistry*, 14 (1), 157–164.

878 Su, Y., Yan, X., Pu, Y., Xiao, F., Wang, D., and Yang, M., 2013. Risks of single-walled carbon nanotubes
879 acting as contaminants-carriers: Potential release of phenanthrene in Japanese medaka
880 (Oryzias latipes). *Environmental Science and Technology*, 47 (9), 4704–4710.

881 Sun, H., Ruan, Y., Zhu, H., Zhang, Z., Zhang, Y., and Yu, L., 2014. Enhanced bioaccumulation of

882 pentachlorophenol in carp in the presence of multi-walled carbon nanotubes. *Environmental*
883 *Science and Pollution Research*, 21 (4), 2865–2875.

884 Sun, T.Y., Bornhöft, N.A., Hungerbühler, K., and Nowack, B., 2016. Dynamic Probabilistic Modeling of
885 Environmental Emissions of Engineered Nanomaterials. *Environmental Science and Technology*,
886 50 (9), 4701–4711.

887 Templeton, R.C., Ferguson, P.L., Washburn, K.M., Scrivens, W.A., and Chandler, G.T., 2006. Life-cycle
888 effects of single-walled carbon nanotubes (SWNTs) on an estuarine meiobenthic copepod.
889 *Environmental Science and Technology*, 40 (23), 7387–7393.

890 VanBerlo, D., Clift, M., Albrecht, C., and Schins, R., 2012. Carbon nanotubes: An insight into the
891 mechanisms of their potential genotoxicity. *Swiss Medical Weekly*, 142 (November), 1–16.

892 Vernon, E.L. and Jha, A.N., 2019. Assessing relative sensitivity of marine and freshwater bivalves
893 following exposure to copper: Application of classical and novel genotoxicological biomarkers.
894 *Mutation Research - Genetic Toxicology and Environmental Mutagenesis*, 842 (January), 60–71.

895 Xia, X., Chen, X., Zhao, X., Chen, H., and Shen, M., 2012. Effects of carbon nanotubes, chars, and ash
896 on bioaccumulation of perfluorochemicals by chironomus plumosus larvae in sediment.
897 *Environmental Science and Technology*, 46 (22), 12467–12475.

898 Xu, H., Cheng, X., Zhong, J., Meng, J., Yang, M., Jia, F., Xu, Z., and Kong, H., 2011. Characterization of
899 multiwalled carbon nanotubes dispersing in water and association with biological effects.
900 *Journal of Nanomaterials*, 2011.

901 Yang, K., Wang, X., Zhu, L., and Xing, B., 2006. Competitive Sorption of Pyrene, Phenanthrene, and
902 Naphthalene on Multiwalled Carbon Nanotubes. *Environmental Science & Technology*, 40 (18),
903 5804–5810.

904 Zangar, R.C., Davydov, D.R., and Verma, S., 2004. Mechanisms that regulate production of reactive
905 oxygen species by cytochrome P450. *Toxicology and Applied Pharmacology*, 199 (3), 316–331.

906 Zhang, S., Zhang, J., Chen, H., Wang, A., Liu, Y., Hou, H. & Hu, Q. (2019). Combined cytotoxicity of co-
907 exposure to aldehyde mixtures on human bronchial epithelial BEAS-2B cells. *Environmental*
908 *Pollution*, 250, 250-261.

909

910

911 **Table 1.** Chemical analyses of the mussel digestive gland after the 3-day exposure to BaP and
912 MWCNTs.

Treatments	Water content (% wet weight)	BaP concentration (µg g^{-1} dry weight)
Solvent control	77.1 ± 2.2	< 0.5
Solvent control + MWCNT 1mg L^{-1}	78.8 ± 2.1	< 0.5
BaP 5 µg L^{-1}	78.7 ± 2.6	6.9 ± 2.1
BaP 50 µg L^{-1}	76.1 ± 1.8	163.2 ± 68.4
BaP 100 µg L^{-1}	75.7 ± 3.8	475.0 ± 45.7
MWCNT + BaP 5 µg L^{-1}	78.0 ± 3.5	6.0 ± 2.6
MWCNT + BaP 50 µg L^{-1}	77.6 ± 3.2	36.1 ± 23.1*
MWCNT + BaP 100 µg L^{-1}	77.9 ± 3.2	267.9 ± 6.4*

913

914 Asterisks indicate the statistical differences observed between treatments exposed to BaP only and
915 treatments exposed to BaP + MWCNTs. (*) $p < 0.05$.

916

917 **Table 2.** Number of DEGs depicted in mussels exposed to BaP alone and with MWCNTs against control (DMSO). Shown are numbers of up- and down-
918 regulated DEGs.

		BaP 5 µg L^{-1}	BaP 50 µg L^{-1}	BaP 100 µg L^{-1}	MWCNT	MWCNT + BaP 5 µg L^{-1}	MWCNT + BaP 50 µg L^{-1}	MWCNT + BaP 100 µg L^{-1}
Gills	**Up**	2	8	6	1	8	6	9
	Down	1	3	3	3	6	4	5
DG	**Up**	7	4	5	3	3	8	4
	Down	7	1	7	1	2	3	1

Table 3. Analysis of combined effects of MWCNT and BaP on DNA Damage (Comet assay) based on Interaction Factors (IF).

Treatments	Interaction Factors for DNA Damage (Comet Assay)
MWCNT 1 mg L^{-1} + BaP 5µg L^{-1}	-396.42 ± 174.57
MWCNT 1 mg L^{-1} + BaP 50 µg L^{-1}	-438.38* ± 297.56
MWCNT 1 mg L^{-1} + BaP 100 µg L^{-1}	-505.92* ± 166.69

Interaction Factor ± 95% Confidence Limit / √2 (Moore et al., 2018). * indicates significance at the 5% level. A negative **IF** indicates antagonism; an **IF** of 0 indicates additivity; and a positive **IF** indicates synergism.

926

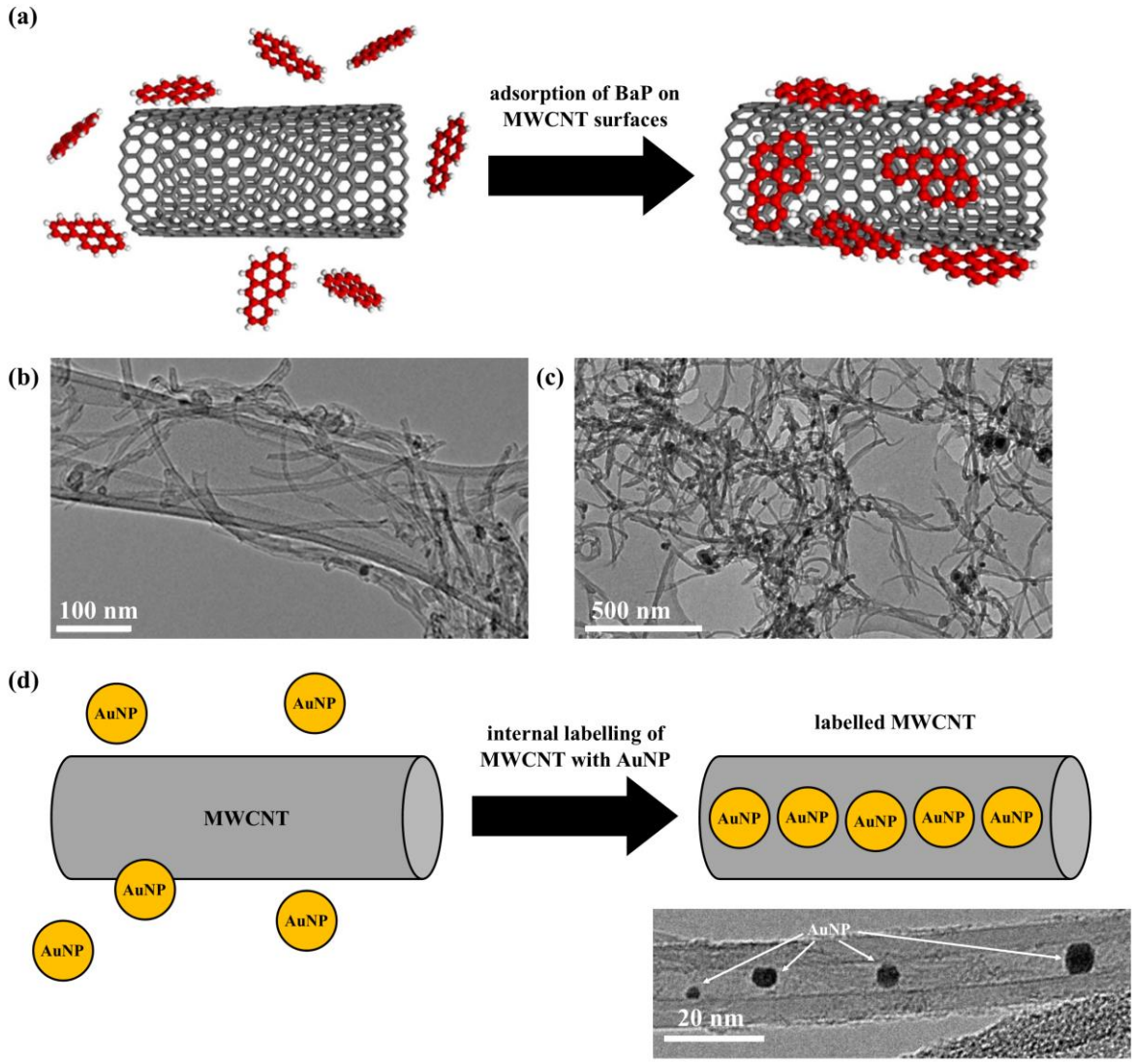

927

928 Figure 1

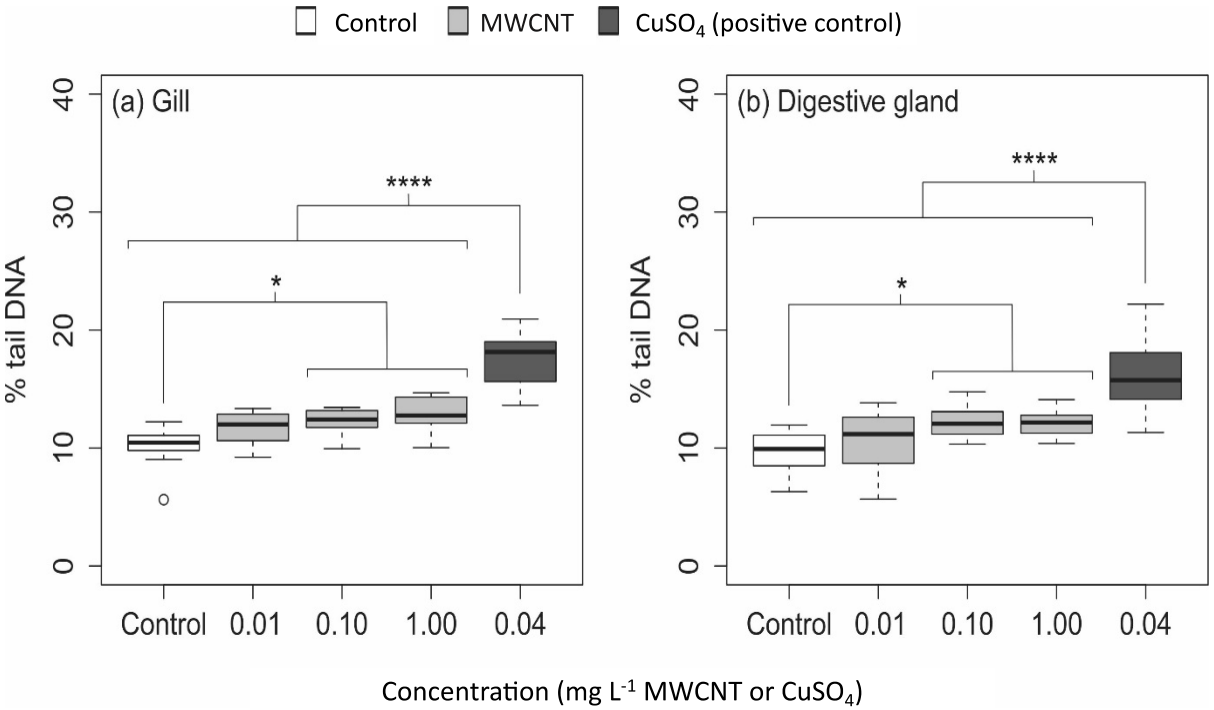

929

930 Figure 2

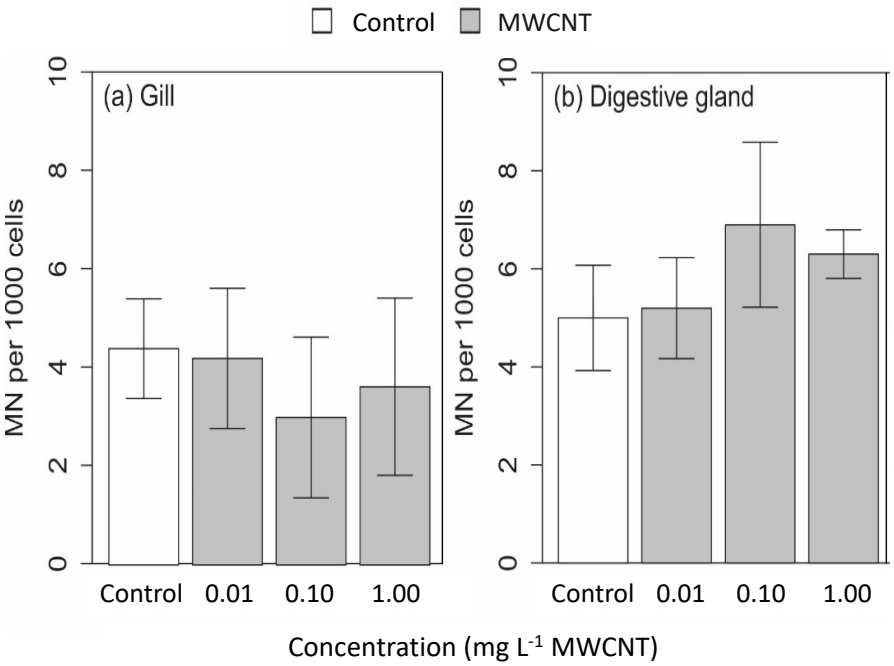

931

932

933 **Figure 3**

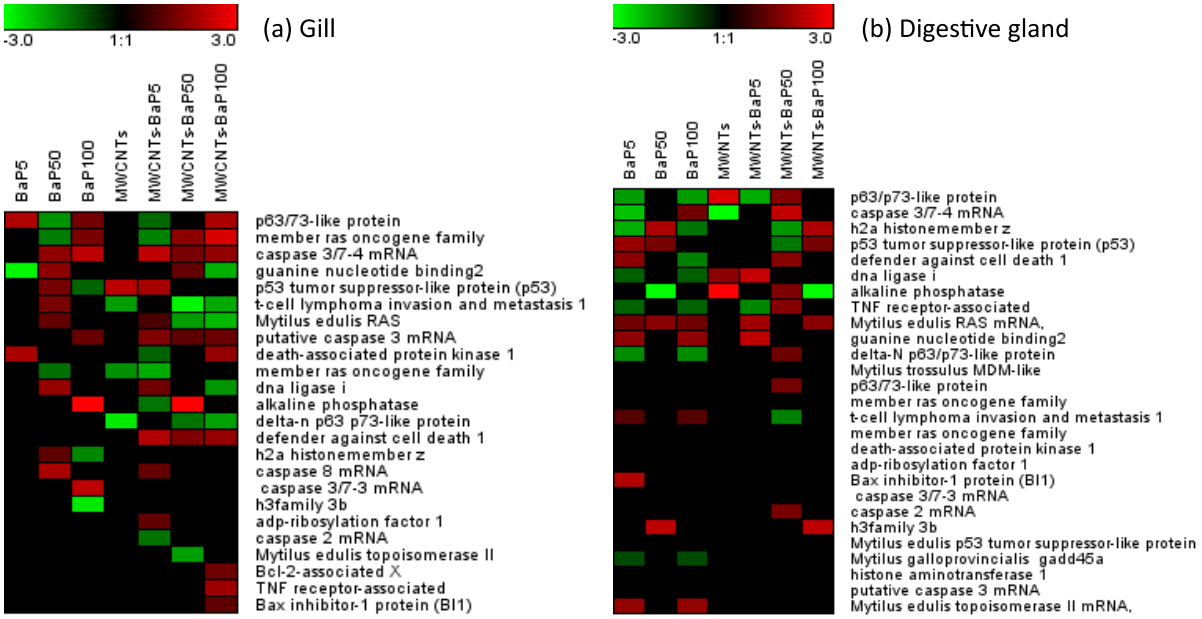
-3.0
1:1
3.0
(a) Gill
BaP5
BaP50
BaP100
MWCNTs
MWCNTs-BaP5
MWCNTs-BaP50
MWCNTs-BaP100
p63/73-like protein
member ras oncogene family
caspase 3/7-4 mRNA
guanine nucleotide binding2
p53 tumor suppressor-like protein (p53)
t-cell lymphoma invasion and metastasis 1
Mytilus edulis RAS
putative caspase 3 mRNA
death-associated protein kinase 1
member ras oncogene family
dna ligase i
alkaline phosphatase
delta-n p63 p73-like protein
defender against cell death 1
h2a histonemember z
caspase 8 mRNA
caspase 3/7-3 mRNA
h3family 3b
adp-ribosylation factor 1
caspase 2 mRNA
Mytilus edulis topoisomerase II
Bcl-2-associated X
TNF receptor-associated
Bax inhibitor-1 protein (BI1)
-3.0
1:1
3.0
(b) Digestive gland
BaP5
BaP50
BaP100
MWNTs
MWNTs-BaP5
MWNTs-BaP50
MWNTs-BaP100
p63/p73-like protein
caspase 3/7-4 mRNA
h2a histonemember z
p53 tumor suppressor-like protein (p53)
defender against cell death 1
dna ligase i
alkaline phosphatase
TNF receptor-associated
Mytilus edulis RAS mRNA,
guanine nucleotide binding2
delta-N p63/p73-like protein
Mytilus trossulus MDM-like
p63/73-like protein
member ras oncogene family
t-cell lymphoma invasion and metastasis 1
member ras oncogene family
death-associated protein kinase 1
adp-ribosylation factor 1
Bax inhibitor-1 protein (BI1)
caspase 3/7-3 mRNA
caspase 2 mRNA
h3family 3b
Mytilus edulis p53 tumor suppressor-like protein
Mytilus galloprovincialis gadd45a
histone aminotransferase 1
putative caspase 3 mRNA
Mytilus edulis topoisomerase II mRNA,

Figure 4

936

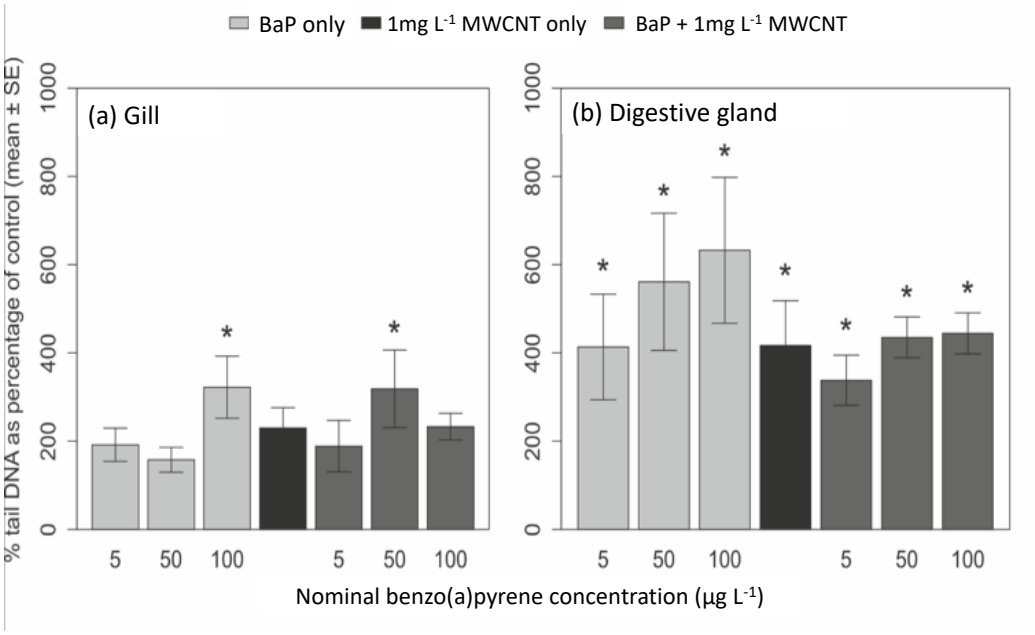

937

938 **Figure 5**

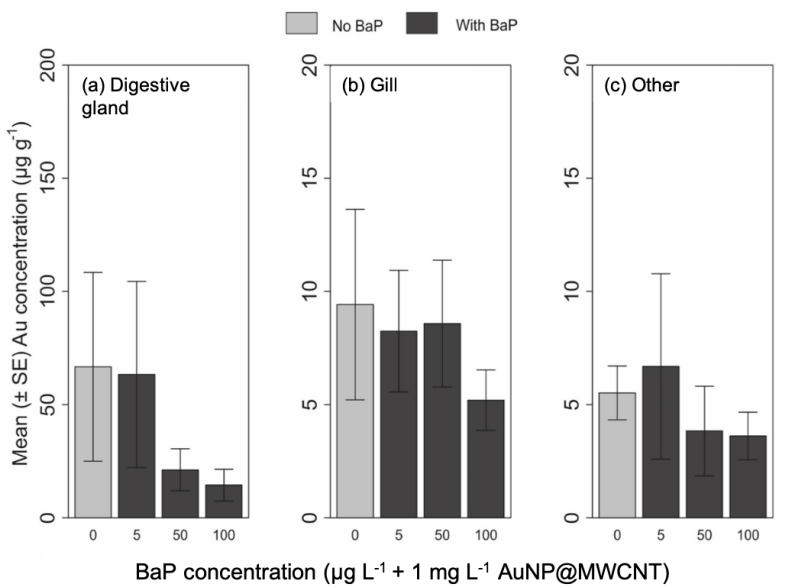

939

940 **Figure 6**

941 **Figure legends and Table captions**

942 **Figure 1.** (a) Schematic diagram illustrating the adsorption of BaP onto the exterior surfaces of
943 MWCNTs due to strong and specific van der Waals interactions. (b) TEM image of MWCNTs used in
944 the experiments with BaP. (c) TEM image of MWCNT aggregates in seawater. In both (b) and (c),
945 aggregated MWCNTs are observed as a consequence of the drying procedure employed during TEM
946 sample preparation; however, MWCNTs appear more aggregated in the presence of seawater, as
947 confirmed by light scattering analysis of the suspension of MWCNTs in seawater (Figure S1). (d)
948 Schematic diagram illustrating the labelling of MWCNTs by insertion of AuNPs into the nanotube
949 cavity that have been employed as diagnostic markers for the presence of MWCNTs in the
950 experiments with BaP. A corresponding TEM image of AuNP@MWCNT with arrows denoting the
951 positions of the confined AuNPs.

952 **Figure 2.** Levels of DNA damage as measured by the Comet assay in the mussel tissues after the 7-
953 day exposure to MWCNTs. Asterisks indicate the statistical differences observed between control
954 and exposed groups. (*) $p < 0.05$, (**) $p < 0.01$, (***) $p < 0.001$.

955 **Figure 3.** Levels of micronuclei in the mussel tissues after the 7-day exposure to MWCNTs.

956 **Figure 4.** Gene expression profile of gill (a) and DG (b) tissues in animals exposed to increasing BaP
957 concentrations (5, 50 and 100 μg L^{-1}) and their combination with MWCNTs (1 mg L^{-1}). The heat map
958 reports log2 relative expression level with respect to the reference condition. 24 and 27 DEGs were
959 generated in at least one condition for gill and DG respectively. Microarray data was analysed using
960 the Linear Mode for Microarray Analysis (LIMMA) software as described in Banni et al, (2011). B
961 statistics with adjusted p-value, 0.05 and B.0 were used as a threshold for rejection of the null
962 hypothesis (no variation).

963 **Figure 5.** Levels of DNA damage as measured by the Comet assay in mussel tissues after 3-day
964 exposure to BaP with and without co-exposure to 1 mg L^{-1} MWCNT. Data are expressed as % control
965 values (not shown) in order to standardise across two different sampling days. Asterisks indicate
966 significant differences from the same tissues in control mussels.

967 **Figure 6.** Gold concentration in mussel (a) gill, (b) DG and (c) other tissues (mean $\pm$ SE) after the 3-
968 day exposure to 1 mg L^{-1} gold-labelled MWCNT (AuNP@MWCNT), with and without co-exposure to
969 BaP. Regarding DG, the highest Au level in the absence and presence of BaP at a concentration of 5

970 µg L^{-1} are due to single outliers. Non-parametric statistical test (Kruskal-Wallis) indicated no
971 significant differences (p-value= 0.3256).

972 **Table 2.** Chemical analyses of the mussel digestive gland after the 3-day exposure to BaP and
973 MWCNTs.

974 **Table 2.** Number of DEGs depicted in mussels exposed to BaP alone and with MWCNTs against
975 control (DMSO). Shown are numbers of up- and down-regulated DEGs.

976 **Table 3**. Analysis of combined effects of MWCNT and BaP on DNA Damage (Comet assay) based on
977 Interaction Factors (IF).

978 **Figure S1.** The hydrodynamic diameter (d_H) of (a) MWCNT in mussel-exposed seawater (1541±193
979 nm), MWCNT in seawater (1666±198 nm) and (c) MWCNT + BaP (1642±431 nm) in mussel-exposed
980 seawater, as determined by DLS. Whilst the maximum possible concentration of MWCNTs in
981 seawater in all experiments is 0.1 mg mL^{-1}, concentrations of the stable suspensions within the range
982 ~0.01-0.02 mg mL^{-1} (~10-20 mg L^{-1}) were determined using a spectrophotometric approach
983 developed within our group previously (Marsh *et al.* 2007), which is an order of magnitude higher
984 than the concentration utilised in the highest exposure experiment, but at the lower limit of the
985 concentration range detectable using the particle sizing instrumentation. The concentration of BaP
986 in seawater in the latter experiment is 0.001 mg mL^{-1}. Control measurements of seawater in the
987 absence of MWCNTs yielded no measurable scatterers.

988 **Figure S2.** (a) TEM and (b) EDX spectroscopy analysis of MWCNTs in seawater. TEM indicates the
989 likelihood of micron-sized MWCNT aggregates in suspension which afford extended web-like
990 ensembles as they deposit onto the carbon films during TEM sample preparation. The EDX spectrum
991 is dominated by C (MWCNT and the grid support film), with smaller signals from Si and O (from silica,
992 a likely contaminant found in seawater). The presence of Cu is associated with the TEM grid and
993 column assembly.

994 **Scheme S1.** Schematic representation of the preparation of AuNP@MWCNT.

995 **Figure S3.** Electron microscopy and *in situ* spectroscopy analysis of AuNP@MWCNT. (a) Bright field
996 TEM image (top) and corresponding STEM/EDX map confirming the presence of Au (bottom). (b) EDX
997 spectra captured from the area shown in (a) indicating the composition of the dark features in the
998 bright field image correspond to AuNPs.

Table S1. The concentration of BaP in seawater at day 1 (1 h after dosing) and day 3 (at the end of the exposure). Data are means ± SE (n = 3) for the BaP 50 treatment.

Table S2: Q-PCR primers and Taqman probes

Table S3: M-Values of DEGs in gills of mussels exposed to increasing BaP concentrations (5 µg L^{-1}, 50 µg L^{-1} and 100 µg L^{-1}) and their combination with MWCNTs (1 mg L^{-1}). Additional information to Figure 4a.

Table S4: M-Values of DEGs in digestive gland of mussels exposed to increasing BaP concentrations (5 µg L^{-1}, 50 µg L^{-1} and 100 µg L^{-1}) and their combination with MWCNTs (1 mg L^{-1}). Additional information to Figure 4b.

Figure S4: Q-PCR confirmation of microarray data. Targets expressions have been analyzed by real-time PCR, using a 18S rRNA, Beta actin and Ribol27 as reference genes for data normalization. Data represent the mean of at least four independent experiments. Calculation of relative expression levels and statistics (pairwise randomization test, $p < 0.05$) were obtained using the REST software (Pfaffl *et al.* 2002). Experimental coefficient of variation (CV) was below 5% for all the investigated targets.

Figure S5. (a,c,e) ESEM imaging and (b,d,f) corresponding point EDX spectroscopy analysis of whole mussel digestive gland tissues. The bright features (which comprise high atomic number elements) in the back scatter ESEM images are used to visually locate nanoscale species of interest. The EDX spectra are collected from these explicit locations and confirm the presence of Ca (b), Fe (d) and Pb (f) as expected environmental contaminants.

Figure S6. (a,c,e) ESEM imaging and (b,d,f) corresponding point EDX spectroscopy analysis of whole mussel digestive gland tissues exposed to AuNP@MWCNT. The EDX spectra confirm the presence of Fe (b,d) and Pt (f) as environmental contaminants. No structures corresponding to labelled MWCNTs were detected either visually or spectroscopically in the whole tissue samples.

Figure S7. (a,c,e) Dark field STEM imaging and (b,d,f) corresponding point EDX spectroscopy analysis of cross-sections of mussel digestive gland. The bright features (which comprise high atomic number elements) in the dark field STEM images are used to visually locate nanoscale species of interest. The EDX spectra are collected from these explicit locations and confirm the presence of Fe (b,f) and silica (d) as expected environmental contaminants.

Figure S8. (a,c,e) Dark field STEM imaging and (b,d,f) corresponding point EDX spectroscopy analysis of cross-sections of mussel digestive gland exposed to AuNP@MWCNT. The EDX spectra confirm the presence of Fe (b), Ag (d) and silica (f) as expected environmental contaminants. No structures corresponding to labelled MWCNTs were detected either visually or spectroscopically in the cross-sections.